# Optical Antennas

Palash Bharadwaj, Bradley Deutsch, and Lukas Novotny*

Institute of Optics and Department of Physics and Astronomy, University of Rochester, Rochester, New York 14627, USA

*Corresponding author: www.nano-optics.org

Optical antennas are an emerging concept in physical optics. Similar to radio-wave and microwave antennas, their purpose is to convert the energy of free propagating radiation to localized energy, and vice versa. Optical antennas exploit the unique properties of metal nanostructures, which behave as strongly coupled plasmas at optical frequencies. The tutorial provides an account of the historical origins and the basic concepts and parameters associated with optical antennas. It also reviews recent work in the field and discusses areas of application, such as light-emitting devices, photovoltaics, and spectroscopy. © 2009 Optical Society of America

OCIS codes: 260.0260, 350.4238, 000.2850, 240.3990.

# Optical Antennas

Palash Bharadwaj, Bradley Deutsch, and Lukas Novotny

## 1. Introduction

In optical science and engineering, light is commonly controlled by redirecting the wave fronts of propagating radiation by means of lenses, mirrors, and diffractive elements. This type of manipulation relies on the wave nature of electromagnetic fields and is therefore not amenable to controlling fields on the subwavelength scale. In contrast, radiowave and microwave technology predominantly makes use of antennas to manipulate electromagnetic fields, controlling them on the subwavelength scale and interfacing efficiently between propagating radiation and localized fields.

While antennas are a key enabling technology for devices like cellular phones and televisions using electromagnetic radiation in the radiowave or microwave regime, their optical analog is basically nonexistent in today's technology. However, recent research in nano-optics and plasmonics has generated considerable interest in the *optical antenna* concept, and several studies are currently focused on how to translate established radiowave and microwave antenna theories into the optical frequency regime.

The absence of optical antennas in technological applications is primarily associated with their small scale. Antennas have characteristic dimensions of the order of a wavelength of light, demanding fabrication accuracies better than 10 nm. The advent of nanoscience and nanotechnology provides access to this length scale with the use of novel top-down nanofabrication tools (e.g. focused ion beam milling and electron-beam lithography) and bottom-up self-assembly schemes. The fabrication of optical antenna structures is an emerging opportunity for novel optoelectronic devices.

Nanotechnology is defined as the application of scientific knowledge to control and utilize matter at the nanometer scale (about $1-100$ nm). At this scale size-related properties and phenomena can emerge [1]. Because diffraction limits the confinement of propagating radiation to roughly half a wavelength, the length scales over which optical fields can be manipulated traditionally lie outside the size range of interest to nanotechnology. It is often possible to spatially separate the nanoscale building blocks and to study their physical and chemical properties by using standard spectroscopic techniques. However, their properties can change once they are embedded in a macroscopic structure because of interactions between the building blocks and with the environment. In fact, one of the most interesting aspects of nanoscale systems involves properties dominated by collective phenomena, which can bring about a large response to a small stimulus in some cases. To understand optical fields in such complex nanoscale struc-

tures, challenging obstacles in detection and control must be overcome. Optical antennas help surpass the diffraction limit, making it possible to manipulate, control, and visualize optical fields on the nanometer scale.

Antennas can enhance several distinct photophysical processes, outlined in Fig. 1. In light-emitting devices, an electron and hole pair combine to emit a photon. The reverse process takes place in photovoltaics, in which incoming light causes a charge separation in a material. In both cases, an optical antenna can be used to couple the propagating field and local electric field, making the transfer of energy between the two more efficient. In spectroscopy, incident light polarizes the material of interest, which generates outgoing radiation. The wavelength of the emitted light is related to the energy-level structure of the material, allowing for chemical identification. In this case, the antenna serves to make both the excitation and the emission more efficient. Antennas are also encountered in biology. In photosynthetic proteins, for example, individual chlorophyll molecules arrange in antenna complexes in order to collectively optimize the efficiency of light absorption.

Given their wide applicability, the absence of optical antennas in current technology is conspicuous. Even as their fabrication becomes feasible, material challenges associated with optical antennas remain. For example, the penetration of radiation into metals can no longer be neglected. The electromagnetic response is then dictated by collective electron oscillations (plasmons) characteristic of a strongly coupled plasma. These collective excitations make a direct downscaling of traditional antenna designs impossible and demand the careful study of surface modes in metal nanostructures.

The introduction of the antenna concept into the optical frequency regime will provide access to new technological applications. Optical antennas will likely be employed to enhance absorption cross sections and quantum yields in photovoltaics, to release energy efficiently from nanoscale light-emitting devices, to boost the efficiency of photochemical or photophysical detectors, and to increase spatial resolution in optical microscopy. In this tutorial, we define the optical antenna, outline its physical properties, and review relevant history and recent work. The field of optical antennas is in its infancy, and new studies and developments are evolving at a rapid pace. Therefore, we do not intend a state-

## Figure 1
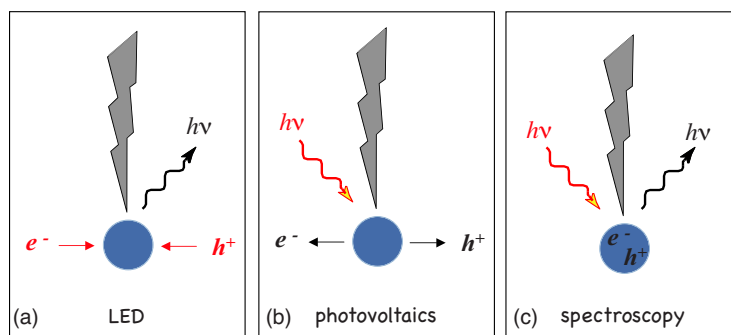


Antenna-based optical interactions: (a) antenna-coupled LED, (b) antenna-coupled photovoltaics, (c) antenna-coupled spectroscopy.

of-the-art review. Rather, we hope to establish language pertaining to optical antennas and to provide historical and future perspectives.

We will begin in Section 2 with a short history of antennas and show how the concept of optical antennas was motivated by microscopy. In Section 3 we derive physical properties of optical antennas in analogy to radiowave or microwave antennas, and we derive several antenna parameters for the example of a spherical nanoparticle. We also discuss wavelength scaling, nonlinear properties of optical antennas, and their effect on atomic or molecular systems. Finally, in Section 4 we outline applications of optical antennas and review some recent developments in the field.

## 2. Antenna History

The word *antenna* has had an interesting history that is worth reviewing. It was first introduced in a translation of Aristotle's writings in 1476 [2]. Aristotle used the Greek word *keraiai* to refer to the "horns" of insects [3], which Theodorus Gaza translated into the Latin-derived *antenna*, used to designate a sailing yard of a lateen. *Antenna* probably derives from the prefix *an*, "up," and the Indo-European root *ten*, "to stretch" [4,5]. The verbs *tan* (Sanskrit), *tendere* (Latin), *teinein* (Greek), *dehnen* (German) and *tyanut'* (Russian), all meaning "to stretch," as well as modern English words such as *tension*, *tent*, *pretend*, *tenacious*, and *tendon* all trace their origins back to this root verb. Etymologically then, an *antenna* is *that which stretches or extends up* [6].

Today, we are accustomed to referring to an electromagnetic transmitter or receiver as an antenna, but these were originally called *aerials* in English [7]. Guglielmo Marconi introduced the term *antenna* in the context of radio in 1895 while performing his first wireless transmission experiments in Salvan, a small town in the Swiss Alps [8]. In Italian, *antennas* denote various kinds of posts, including those of tents or ships. Since Marconi's father Giuseppe had encouraged him to become a naval officer, he was familiar with the nautical term, and likely introduced it in the electromagnetic sense as an analogy [9].

Evidence suggests that the term *antenna* first found only casual verbal use in English, and that it took about a decade before it was popularly used in scientific work. Marconi did not refer to antennas in his patents, but he makes use of the term in his Nobel Prize speech of 1909 [10]. The term can also be found in George W. Pierce's article of 1904 [11] and in John A. Fleming's 1902 entry in the *Encyclopedia Britannica XXXIII* referring to Marconi's work [12].

The first document we are aware of that uses the word *antenna* for an electromagnetic transmitter is a paper by André-Eugène Blondel titled "Sur la théorie des antennes dans la télégraphie sans fil," presented in 1898 at a meeting of the *Association Française pour l'Avancement des Sciences*. Blondel, the inventor of the oscillograph, also refers to antennas in a letter that he sent to H. Poincaré in August 1898 [13]. We also find the term *antenna* in the book by André Broca titled *La télégraphie sans fils* published in French in 1899 [14]. Broca states that an antenna is a means for concentrating electromagnetic waves and defines it as "the vertical long-wire pole of an excitation source." The other pole is considered to be grounded. He writes that "the extremity of the antenna is a point of escape for electromagnetic energy" and that an antenna is also needed on the receiving end, similar to Benjamin Franklin's lightning rod [15]. The term *antenna*

is also used in a 1900 French patent by Manuel Rodriguez Garcia [16] and in subsequent U.S. patents filed in 1901 [17,18].

In 1895 Marconi described his experiments to his friend Luigi Solari, a Navy lieutenant: "… by chance I was keeping one of the metal plates at a very high distance from the ground while the other one was in the ground. Using this arrangement the signals became so strong that I was able to transmit up to one kilometer away. From that moment on the progress increased enormously. The plate at the top—the antenna—was raised more and more and the other one—the terra—was buried in the ground." [9] Various antenna geometries have been developed since and many books have been written on antenna theory. In 1983, IEEE defined the antenna as "a means for radiating or receiving radio waves" (IEEE Std 145-1983) [19].

## 2.1. Optical Antennas

While radio antennas were developed as solutions to a communication problem, the invention of optical antennas was motivated by microscopy. In analogy to its radiowave and microwave counterparts, we define the *optical antenna* as a device designed to efficiently convert free-propagating optical radiation to localized energy, and vice versa. In the context of microscopy, an optical antenna effectively replaces a conventional focusing lens or objective, concentrating external laser radiation to dimensions smaller than the diffraction limit.

> *Optical antenna: a device designed to efficiently convert free-propagating optical radiation to localized energy, and vice versa.*

In a letter dated April 22, 1928, Edward Hutchinson Synge described to Albert Einstein a microscopic method in which the field scattered from a tiny particle could be used as a light source [20]. The particle would convert free-propagating optical radiation into a localized field that would interact with a sample surface. Thinking of the surface as a receiver, the particle can be viewed as an optical antenna. Synge's description was likely inspired by the development of dark-field microscopy, a technique invented at the turn of the twentieth century by the Austrian chemist Richard Adolf Zsigmondy [21].

John Wessel was unfamiliar with Synge's work when he wrote in 1985, "The particle serves as an antenna that receives an incoming electromagnetic field [22]," making him the first to mention explicitly the analogy of local microscopic light sources to classical antennas—a concept that has since been thoroughly explored [23,24]. The invention of scanning tunneling microscopy [25] and the discovery of surface enhanced Raman scattering (SERS) [26–28] most likely inspired Wessel's idea. The quest for an understanding of SERS gave rise to many theoretical studies aimed at predicting the electromagnetic field enhancement near laser-irradiated metal particles and clusters [29–33]. This era can be considered the first phase of what is now called *nanoplasmonics*. In 1988 Ulrich Ch. Fischer and Dieter W. Pohl carried out an experiment similar to Synge's and Wessel's proposals [34]. Instead of a solid metal particle, they used a gold-coated polystyrene particle as a local light source, a structure that was later extensively developed and is now called a *gold nanoshell* [35,36]. Fischer and

Pohl imaged a thin metal film with 320 nm holes and demonstrated a spatial resolution of ~50 nm. Their results provide the first experimental evidence that near-field scanning optical microscopy as introduced by Synge is feasible. Ten years later, laser-irradiated metal tips were proposed as optical antenna probes for near-field microscopy and optical trapping [37,38], and since then various antenna geometries have been studied (rods, bowties, etc.), some of which are reviewed below.

The optical antenna concept also has strong parallels with the development of so-called whisker diodes in the 1960s. An antenna attached to a metal-to-metal point contact was used in 1968 by Ali Javan and co-workers for frequency mixing of IR radiation [39]. It was shown that the rectification efficiency of these whisker diodes could be increased by suitably "kinking," or bending the wire antenna [40]. The length $L$ (tip to kink) had to be adjusted in relation to the wavelength and angle of incidence, and the strongest response was obtained for the fundamental resonance of $L \approx \lambda/2.7$ [41]. These experiments were performed at IR wavelengths, at which metals are good conductors. IR antenna fabrication has expanded considerably in the past few decades, notably including work by Glen Boreman, who since the late 1990s has fabricated many types for use in IR detectors, bolometers, and nanophotonics [42–44]. Figure 2 catalogs several examples of these antennas. In search of a near-field optical probe with a higher efficiency than tapered fibers, in 1997 Robert Grober tested a microwave-scale model of a bowtie antenna at the end of a waveguide [48] and demonstrated confinement of a tenth of a wavelength ($\lambda$) with 30% transmission efficiency. He
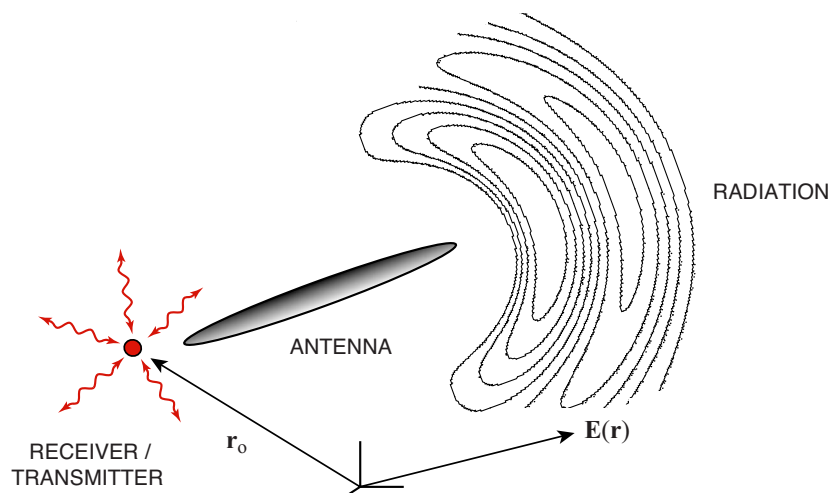
## Figure 2
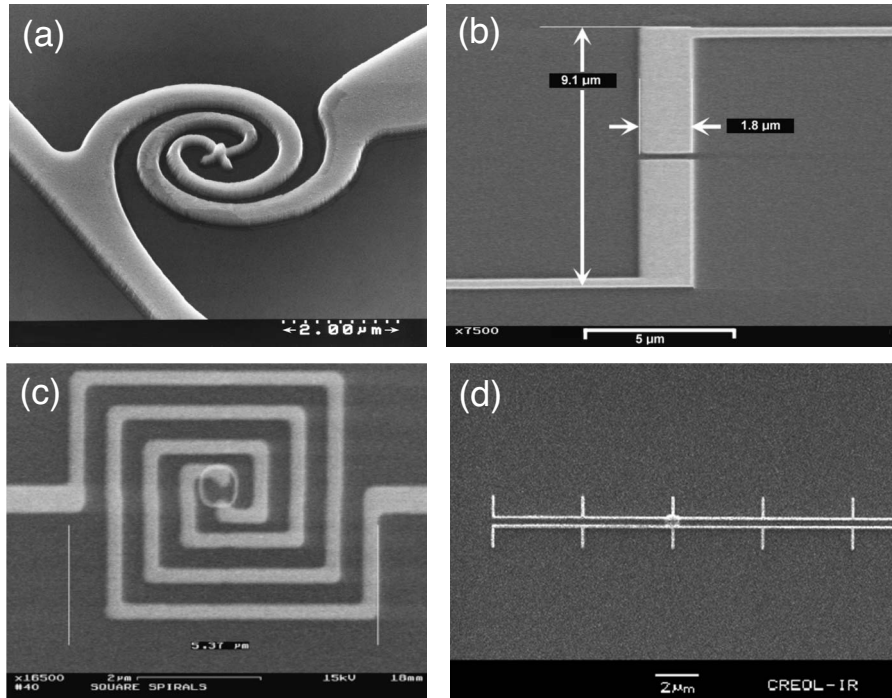


Examples of IR optical antennas fabricated by Boreman and co-workers: (a) asymmetric spiral antenna [45], (b) microstrip dipole antenna [46], (c) square spiral antenna [43], (d) phased-array antenna [47].

Problem statement of optical antenna theory. A receiver or transmitter (atom, ion, molecule...) interacts with free optical radiation via an optical antenna.

suggested that such antennas could be fabricated for visible frequencies, which motivated several independent experimental efforts.

## 3. Physical Properties of Optical Antennas

Optical antennas are strongly analogous to their RF and microwave counterparts, but there are crucial differences in their physical properties and scaling behavior. Most of these differences arise because metals are not perfect conductors at optical frequencies, but are instead strongly correlated plasmas described as a free electron gas. Optical antennas are also not typically driven with galvanic transmission lines—localized oscillators are instead brought close to the feed point of the antennas, and electronic oscillations are driven capacitively [49]. Moreover, optical antennas can take various unusual forms (tips, nanoparticles, etc.) and their properties may be strongly shape and material dependent owing to surface plasmon resonances.

The general problem statement of optical antenna theory is illustrated in Fig. 3. A receiver or transmitter interacts with free optical radiation via an optical antenna. The receiver or transmitter is ideally an elemental quantum absorber or emitter, such as an atom, ion, molecule, quantum dot, or defect center in a solid. The antenna enhances the interaction between the emitter or absorber and the radiation field. It therefore provides the prospect of controlling the light–matter interaction on the level of a single quantum system. The presence of the antenna modifies the properties of the receiver/transmitter, such as its transition rates and, in the case of a strong interaction, even the energy-level structure. Likewise, the antenna properties depend on those of the receiver–transmitter, and it becomes evident that the two must be regarded as a coupled system. In this section, we will address these issues and attempt to express them in terms of established antenna terminology.

## 3.1. Local Density of Electromagnetic States

Arguably, one of the most important quantities in a discussion of antennas is the impedance, defined in circuit theory in terms of source current $I$ and voltage $V$ as $Z = V/I$. This definition assumes that the source is connected to the antenna via a current-carrying transmission line. But optical antennas are typically fed by localized light emitters, not by real currents. Thus, the definition of antenna input impedance needs some adjustments. A viable alternate definition involves the local density of electromagnetic states (LDOS), which can be expressed in terms of the Green's function tensor $\overset{\leftrightarrow}{G}$ and which accounts for the energy dissipation of a dipole in an arbitrary inhomogeneous environment.

Single emitters such as atoms and molecules are inherently quantum objects that, strictly speaking, demand a quantum mechanical treatment. However, a two-level system that mostly resides in the ground state (perturbation limit) can be represented by a classical dipole [50]. Therefore, we begin the discussion with the quantum mechanical description of a two-level atom and then establish the link to the classical representation.

The total decay rate of a two-level quantum emitter located at $\mathbf{r}_o$ and weakly coupled to the antenna can be represented by Fermi's golden rule as [51]

$$\Gamma = \frac{\pi\omega}{3\hbar\varepsilon_o}|\langle g|\hat{\mathbf{p}}|e\rangle|^2 \rho_{\mathbf{p}}(\mathbf{r}_o,\omega),\tag{1}$$

where $\langle g|\hat{\mathbf{p}}|e\rangle$ is the transition dipole moment between the emitter's excited state $|e\rangle$ and ground state $|g\rangle$, $\omega$ is the transition frequency, and $\rho_{\mathbf{p}}$ denotes the *partial* density of electromagnetic states (LDOS). The latter can be expressed in terms of the system's dyadic Green's function $\overset{\leftrightarrow}{G}$ as [51,52]

$$\rho_{\mathbf{p}}(\mathbf{r}_o,\omega) = \frac{6\omega}{\pi c^2}[\mathbf{n}_p \cdot \text{Im}\{\overset{\leftrightarrow}{G}(\mathbf{r}_o,\mathbf{r}_o,\omega)\} \cdot \mathbf{n}_p],\tag{2}$$

where $\mathbf{n}_p$ is a unit vector pointing in direction of $\mathbf{p}$. The Green's function used in Eq. (2) is indirectly defined by the electric field $\mathbf{E}$ at the observation point $\mathbf{r}$ generated by a dipole $\mathbf{p}$ located at $\mathbf{r}_o$,

$$\mathbf{E}(\mathbf{r}) = \frac{1}{\varepsilon_o}\frac{\omega^2}{c^2}\overset{\leftrightarrow}{G}(\mathbf{r},\mathbf{r}_o,\omega)\mathbf{p}.\tag{3}$$

Notice that the Green's function in Eq. (2) is evaluated at $\mathbf{r}_o$, which is the position of the emitter itself. This reflects the fact that the decay from the excited state happens in response to the emitter's own field.

The *total* LDOS ($\rho$) is obtained by assuming that the quantum emitter has no preferred dipole axis (atom). Averaging Eq. (2) over different dipole orientations leads to

$$\rho(\mathbf{r}_o,\omega) = \langle\rho_{\mathbf{p}}(\mathbf{r}_o,\omega)\rangle = \frac{2\omega}{\pi c^2}\text{Im}\{Tr[\overset{\leftrightarrow}{G}(\mathbf{r}_o,\mathbf{r}_o,\omega)]\},\tag{4}$$

where $Tr$ denotes the trace. Thus, the excited state lifetime $\tau = 1/\Gamma$ of the quantum emitter is determined by the Green's function $\overset{\leftrightarrow}{G}$ of the system in which the emitter is embedded. The LDOS therefore accounts for the presence of the an-

tenna and is a measure of its properties. In free space, i.e., in the absence of the antenna, we obtain $\rho_{\mathbf{p}} = \omega^2/(\pi^2 c^3)$ and $\Gamma_o = \omega^3 |\langle g|\hat{\mathbf{p}}|e\rangle|^2/(3\pi\varepsilon_o\hbar c^3)$. The observation that atomic decay rates are dependent on the local environment goes back to Purcell's analysis in 1946 [53] and has since been measured for various systems, such as molecules near interfaces [54] or atoms in cavities [55,56]. The origin for the modification of atomic decay rates is the interaction of the atom with its own secondary field—the field that arrives back at the atom's location after being scattered in the local environment. This back-action also influences the energy states and transition frequencies [57,58], but the effect is generally much smaller than the modification of transition rates.

## 3.2. Power Dissipation and Antenna Impedance

The Green's function introduced in the previous section corresponds to the electric field of a classical dipole oscillating at frequency $\omega$ [59]. We likewise represent the quantum emitter by a classical dipole $\mathbf{p}$, a pointlike source current located at $\mathbf{r}_o$. According to Poynting's theorem the power dissipated by a time-harmonic system is

$$P = \frac{1}{2}\int_V \mathrm{Re}\{\mathbf{j}^* \cdot \mathbf{E}\}dV, \tag{5}$$

where $V$ is the source volume, $\mathbf{j}$ the current density, and $\mathbf{E}$ the electric field. The current density $\mathbf{j}$ can be expanded in a Taylor series around some origin $\mathbf{r}_o$ and to lowest approximation can be written as

$$\mathbf{j}(\mathbf{r}) = -i\omega\mathbf{p}\,\delta[\mathbf{r} - \mathbf{r}_o], \tag{6}$$

where $\mathbf{p}$ is the dipole moment and $\delta$ the Dirac delta function. Insertion into Eq. (5) yields

$$P = \frac{\omega}{2}\,\mathrm{Im}\{\mathbf{p}^* \cdot \mathbf{E}(\mathbf{r}_o)\}. \tag{7}$$

The electric field in this expression is the field generated by the dipole and evaluated at the dipole's origin. Expressing the field in terms of the Green's function according to Eq. (3), we obtain for the dissipated power

$$P = \frac{\pi\omega^2}{12\varepsilon_o}|\mathbf{p}|^2\rho_{\mathbf{p}}(\mathbf{r}_o,\omega), \tag{8}$$

where we used Eq. (2) for $\rho_{\mathbf{p}}$. Using the known expression for dipole radiation in free space, $P^o = |\mathbf{p}|^2\omega^4/(12\pi\varepsilon_o c^3)$, we can express the LDOS in terms of the normalized power radiation

$$\rho_{\mathbf{p}}(\mathbf{r}_o,\omega) = \frac{\omega^2}{\pi^2 c^3}P/P^o. \tag{9}$$

The factor $\omega^2/(\pi^2 c^3)$ corresponds to the LDOS in free space and is used in the standard derivation of blackbody radiation.

Comparing Eqs. (1) and (8) we find the interesting result that

$$\frac{\mathrm{P}}{\Gamma} = \frac{|\mathbf{p}|^2}{|\langle g|\hat{\mathbf{p}}|e\rangle|^2} \frac{\hbar\omega}{4}. \tag{10}$$

The ratio of power dissipation to the transition rate can be expressed in terms of the dipole moments. Failing to distinguish between the transition dipole and classical dipole leads to the erroneous result $\mathrm{P} = (\Gamma/4)\hbar\omega$, in which $\Gamma$ represents a photon emission rate. However, $\Gamma$ is **not** the photon emission rate, but the transition rate between the initially excited electronic state $|e\rangle$ and the electronic ground state $|f\rangle$. The advantage in using the LDOS now becomes clear: it allows for a safe link between quantum and classical formalisms.

We now return to the circuit-theory definition of the impedance. The antenna resistance follows from the dissipated power according to $\mathrm{Re}\{Z\} = \mathrm{P}/I^2$. Since we have a driving dipole instead of a physical current, it is more useful to define $Z$ in terms of the current density, $\mathbf{j} \sim i\omega\mathbf{p}$, instead of the current, $I$. Equation (8) thus yields [60]

$$\mathrm{Re}\{Z\} = \frac{\pi}{12\varepsilon_o} \rho_p(\mathbf{r}_o, \omega). \tag{11}$$

Hence, the LDOS can be associated with the antenna resistance $\mathrm{Re}\{Z\}$. The units of such a resistance are ohms per area instead of the usual ohms. Notice that $Z$ depends on both the location $\mathbf{r}_o$ and the orientation $\mathbf{n}_p$ of the receiving or transmitting dipole. As discussed by Greffet *et al.* [60], the imaginary part of $Z$ accounts for the energy stored in the near field.

## 3.3. Antenna Efficiency, Directivity, and Gain

The power P in Eq. (8) accounts for the total dissipated power, which is the sum of radiated power $\mathrm{P_{rad}}$ and power dissipated into heat and other channels ($\mathrm{P_{loss}}$). The antenna radiation efficiency $\varepsilon_{\mathrm{rad}}$ is defined as

$$\varepsilon_{\mathrm{rad}} = \frac{\mathrm{P_{rad}}}{\mathrm{P}} = \frac{\mathrm{P_{rad}}}{\mathrm{P_{rad}} + \mathrm{P_{loss}}}. \tag{12}$$

While P is most conveniently determined by calculating the field $\mathbf{E}$ at the dipole's position according to Eq. (7), $\mathrm{P_{rad}}$ requires the calculation of the energy flux through a surface enclosing both the dipole and the antenna.

It is useful to distinguish dissipation in the antenna and the transmitter, which is not accomplished by Eq. (12). We therefore define the intrinsic quantum yield of the emitter as

$$\eta_i = \frac{\mathrm{P_{rad}^o}}{\mathrm{P_{rad}^o} + \mathrm{P_{intrinsic\ loss}^o}}, \tag{13}$$

where the superscripts $o$ designate the absence of the antenna. With this definition of $\eta_i$ we can rewrite Eq. (12) as

$$\varepsilon_{rad} = \frac{P_{rad}/P_{rad}^o}{P_{rad}/P_{rad}^o + P_{antenna\ loss}/P_{rad}^o + [1 - \eta_i]/\eta_i}. \tag{14}$$

For an emitter with $\eta_i = 1$ (no intrinsic loss) the antenna can only reduce the efficiency. However, for emitters with low $\eta_i$ we can effectively increase the overall efficiency, which holds promise for the optimization of light emitting devices.

To account for the angular distribution of the radiated power we define the normalized angular power density $p(\theta, \varphi)$, or radiation pattern, as

$$\int_0^\pi \int_0^{2\pi} p(\theta, \varphi)\sin\theta d\varphi d\theta = P_{rad}. \tag{15}$$

The directivity $D$ is a measure of an antenna's ability to concentrate radiated power into a certain direction. It corresponds to the angular power density relative to a hypothetical isotropic radiator. Formally,

$$D(\theta, \varphi) = \frac{4\pi}{P_{rad}}p(\theta, \varphi). \tag{16}$$

When the direction $(\theta, \varphi)$ is not explicitly stated, one usually refers to the direction of maximum directivity, i.e., $D_{max} = (4\pi/P_{rad})\text{Max}[p(\theta, \varphi)]$.

Because the fields at a large distance from an antenna are transverse, they can be written in terms of two polarization directions, $\mathbf{n}_\theta$ and $\mathbf{n}_\varphi$. The partial directivities are then defined as

$$D_\theta(\theta, \varphi) = \frac{4\pi}{P_{rad}}p_\theta(\theta, \varphi), \quad D_\varphi(\theta, \varphi) = \frac{4\pi}{P_{rad}}p_\varphi(\theta, \varphi). \tag{17}$$

Here, $p_\theta$ and $p_\varphi$ are the normalized angular powers measured after polarizers aligned in direction $\mathbf{n}_\theta$ and $\mathbf{n}_\varphi$, respectively. Because $\mathbf{n}_\theta \cdot \mathbf{n}_\varphi = 0$, we have

$$D(\theta, \varphi) = D_\theta(\theta, \varphi) + D_\varphi(\theta, \varphi). \tag{18}$$

The influence of an optical antenna on the radiation pattern of a single molecule was recently studied by van Hulst and co-workers [61–64], and it was shown that the antenna provides a high level of control for the direction and polarization of the emitted photons.

The gain $G$ of an antenna follows a definition similar to that of the directivity, but instead of normalizing with the radiated power $P_{rad}$ the gain is defined relative to the total power P, i.e.,

$$G = \frac{4\pi}{P}p(\theta, \varphi) = \varepsilon_{rad}D. \tag{19}$$

$D$ and $G$ are usually measured in decibels. Since perfectly isotropic radiators do not exist in reality, it is often more practical to refer to an antenna of a known directional pattern. The *relative gain* is then defined as the ratio of the power gain in a given direction to the power gain of a reference antenna in the same direction. A dipole antenna is the standard choice as a reference because of its relatively simple radiation pattern. Bouhelier and co-workers recently characterized the relative gain of optical antennas made from metal nanoparticle dimers, using as a reference the dipolelike radiation from single nanoparticles [65].

## 3.4. Radiative Enhancement

The reciprocity theorem states that for a closed system (no incoming waves) with two separable and finite-sized current distributions $\mathbf{j}_1$ and $\mathbf{j}_2$, producing the fields $\mathbf{E}_1$ and $\mathbf{E}_2$, respectively, the following relationship holds [66]:

$$\int_V \mathbf{j}_1 \cdot \mathbf{E}_2 dV = \int_V \mathbf{j}_2 \cdot \mathbf{E}_1 dV. \tag{20}$$

According to Eq. (6), for two dipoles this equation simplifies to

$$\mathbf{p}_1 \cdot \mathbf{E}_2 = \mathbf{p}_2 \cdot \mathbf{E}_1. \tag{21}$$

We will use this equation to derive a relationship between the excitation rate $\Gamma_{\text{exc}}$ of dipole $\mathbf{p}_1$ and its radiative rate $\Gamma_{\text{rad}}$, following the steps used by Taminiau *et al.* [67,68].

Let us consider the situation depicted in Fig. 4 in which one dipole ($\mathbf{p}_1$) represents a quantum emitter or absorber near an optical antenna and the other dipole ($\mathbf{p}_2$) is a dummy dipole representing the location of a point detector. The separation between the two dipoles is assumed to be sufficiently large ($kR \gg 1$) to ensure that they interact only via their far fields. Furthermore, the direction of $\mathbf{p}_2$ is chosen to be transverse to the vector connecting the two dipoles.

In the classical picture, we assume that dipole $\mathbf{p}_1$ has been induced by the field $\mathbf{E}_2$ of dipole $\mathbf{p}_2$ according to $\mathbf{p}_1 = \overleftrightarrow{\alpha}_1 \mathbf{E}_2$, where $\overleftrightarrow{\alpha}_1 = \alpha_1 \mathbf{n}_{\mathbf{p}_1} \mathbf{n}_{\mathbf{p}_1}$ is the polarizability tensor. Here, $\mathbf{n}_{\mathbf{p}_1}$ is the unit vector in the direction of $\mathbf{p}_1$. According to Eq. (7), the power absorbed by the particle at $\mathbf{r}_1$ is

$$P_{\text{exc}} = (\omega/2)\text{Im}\{\mathbf{p}_1^* \cdot \mathbf{E}_2(\mathbf{r}_1)\} = (\omega/2)\text{Im}\{\alpha_1\}|\mathbf{n}_{\mathbf{p}_1} \cdot \mathbf{E}_2(\mathbf{r}_1)|^2. \tag{22}$$

We now substitute reciprocity relation (21) in the form $p_1 \mathbf{n}_{\mathbf{p}_1} \cdot \mathbf{E}_2 = p_2 \mathbf{n}_{\mathbf{p}_2} \cdot \mathbf{E}_1$ and obtain

$$P_{\text{exc}} = (\omega/2)|p_2/p_1|^2 \, \text{Im}\{\alpha_1\}|\mathbf{n}_{\mathbf{p}_2} \cdot \mathbf{E}_1(\mathbf{r}_2)|^2. \tag{23}$$

The term $|\mathbf{n}_{\mathbf{p}_2} \cdot \mathbf{E}_1(\mathbf{r}_2)|^2$ corresponds to the power a photodetector at $\mathbf{r}_2$ would read if it were placed behind a polarizer oriented in direction $\mathbf{n}_{\mathbf{p}_2}$.

We now invoke the partial directivities defined in Eqs. (17). In terms of the field $\mathbf{E}$ evaluated at $\mathbf{r}_2 = (R, \theta, \varphi)$ the partial directivity $D_\theta$ reads as
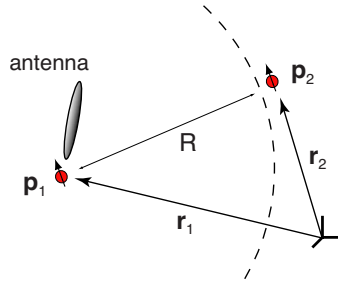


Figure 4

Illustration of reciprocity between two point emitters. The excitation rate $\Gamma_{\text{exc}}$ of $\mathbf{p}_1$ is related to its radiative decay rate $\Gamma_{\text{rad}}$ and its directivity $D(\theta, \varphi)$.

$$D_\theta(\theta,\varphi) = 4\pi \frac{\left| \mathbf{n}_\theta \cdot \mathbf{E}(R,\theta,\varphi) \right|^2}{\displaystyle\int_{4\pi} \left| \mathbf{E}(R,\theta,\varphi) \right|^2 d\Omega}, \tag{24}$$

where $\Omega$ is the unit solid angle and $\mathbf{n}_\theta$ the unit polar vector. $D_\varphi(\theta,\varphi)$, referring to radiation polarized in azimuthal direction $\mathbf{n}_\varphi$, is expressed similarly.

To proceed, we choose the dipole $\mathbf{p}_2$ to point in direction of $\mathbf{n}_\theta$. Equation (23) can then be represented as

$$P_{\mathrm{exc},\theta}(\theta,\varphi) = (\omega/2)\left| p_2/p_1 \right|^2 \mathrm{Im}\{\alpha_1\} \frac{P_{\mathrm{rad}}}{2\pi\varepsilon_o c R^2} D_\theta(\theta,\varphi). \tag{25}$$

Here, $P_{\mathrm{rad}} = (1/2)\varepsilon_o c R^2 \int_{4\pi} |\mathbf{E}(R,\theta,\varphi)|^2 d\Omega$ is the total radiated power. The left-hand side, $P_{\mathrm{exc},\theta}(\theta,\varphi)$, specifies the power absorbed by dipole $\mathbf{p}_1$ when it is excited by the field of dipole $\mathbf{p}_2$ located at $(R,\theta,\varphi)$ and oriented in the $\mathbf{n}_\theta$ direction. Because $kR \gg 1$, the field exciting dipole $\mathbf{p}_1$ and the antenna is essentially a plane wave polarized in $\mathbf{n}_\theta$.

We now remove the antenna and write an equation similar to Eq. (25). Dividing the two equations yields

$$\frac{P_{\mathrm{exc},\theta}(\theta,\varphi)}{P^o_{\mathrm{exc},\theta}(\theta,\varphi)} = \frac{P_{\mathrm{rad}}}{P^o_{\mathrm{rad}}} \frac{D_\theta(\theta,\varphi)}{D^o_\theta(\theta,\varphi)}, \tag{26}$$

where the superscript $o$ carries the same meaning as in Eq. (15). Invoking the proportionality Eq. (10) between power P and transition rate $\Gamma$, we can represent the above equation as

$$\frac{\Gamma_{\mathrm{exc},\theta}(\theta,\varphi)}{\Gamma^o_{\mathrm{exc},\theta}(\theta,\varphi)} = \frac{\Gamma_{\mathrm{rad}}}{\Gamma^o_{\mathrm{rad}}} \frac{D_\theta(\theta,\varphi)}{D^o_\theta(\theta,\varphi)}, \tag{27}$$

which states that the enhancement of the excitation rate due to the presence of the antenna is proportional to the enhancement of the radiative rate, a relationship that has been used qualitatively in various studies [67,69–71]. Note that the same analysis can be repeated with $\mathbf{n}_\varphi$ instead of $\mathbf{n}_\theta$, which corresponds to polarization rotated by 90°.

In most experiments, a quantum emitter is excited by focused laser radiation rather than a polarized plane wave from $(\theta,\varphi)$. In this case, the incident field can be written as an angular spectrum of plane waves and their mutual interferences accounted for to arrive at a correct relationship between $\Gamma_{\mathrm{exc}}$ and $\Gamma_{\mathrm{rad}}$.

## 3.5. Antenna Aperture and Absorption Cross Section

The antenna aperture or effective area, $A$, describes the efficiency with which incident radiation is captured. It corresponds to the area of incident radiation that interacts with the antenna and is defined as

$$A(\theta,\varphi,\mathbf{n}_{\mathrm{pol}}) = \frac{P_{\mathrm{exc}}}{I} = \sigma_A(\theta,\varphi,\mathbf{n}_{\mathrm{pol}}), \tag{28}$$

where $P_{\mathrm{exc}}$ denotes the power that excites the receiver and $I$ is the intensity of radiation incident from $(\theta,\varphi)$ and polarized in direction $\mathbf{n}_{\mathrm{pol}}$. If the direction or

polarization is not specified, one usually refers to that which yields the maximum aperture. Formally, $A$ is equivalent to the absorption (or excitation) cross section $\sigma_A$.

In the absence of the antenna, the absorption cross section of a two-level system has a theoretical limit of $\sigma_o = 3\lambda^2/(2\pi)$ [72]. Typical values for dye molecules or quantum dots are of the order of $\sigma_o \sim 1$ nm$^2$. Thus, a planar array of molecules with nearest neighbor distances of $\sim 1$ nm would interact with all of the incident radiation.

The antenna increases the optical energy density that falls on a target and thereby increases its efficiency. For example, the overall efficiency of a photodetector can be improved when coupled to an optical antenna [73]. For a detector small compared with the wavelength $\lambda$ the received power is calculated according to Eqs. (7) and (22) as

$$P_{exc} = (\omega/2)\text{Im}\{\alpha\}|\mathbf{n}_p \cdot \mathbf{E}|^2. \tag{29}$$

Here, $\mathbf{n}_p$ is the unit vector in the direction of the absorption dipole $\mathbf{p}$, and $\mathbf{E}$ is the field at the location of the detector. If we denote the field at the target in the absence of the antenna as $\mathbf{E}_o$, we can represent the absorption cross section (antenna aperture) as

$$\sigma = \sigma_o|\mathbf{n}_p \cdot \mathbf{E}|^2/|\mathbf{n}_p \cdot \mathbf{E}_o|^2. \tag{30}$$

Here, $\sigma_o$ is the absorption cross section in the absence of the antenna and $\mathbf{E}$ is the field at the target in presence of the antenna. Note that both $\sigma$ and $\sigma_o$ depend on the direction of incidence $(\theta, \varphi)$ and the polarization direction $\mathbf{n}_{pol}$. According to Eq. (30) the enhancement of the absorption cross section, and aperture, corresponds to the local intensity enhancement factor.

Several studies have demonstrated that intensity enhancements of $10^4 \dots 10^6$ are feasible [37,74,75]. Using these values as working numbers we find that by use of optical antennas the areal density of discrete absorbers can be reduced by 4–6 orders of magnitude without sacrificing any loss of absorption. For example, a planar solar cell consisting of an array of antenna-coupled molecules or quantum dots spaced by 100 nm to 1 $\mu$m would interact with all of the incident radiation.

## 3.6. Example: Nanoparticle Antenna

Let us consider a spherical nanoparticle as a simple example of an optical antenna [23,24,71,76,77]. The nanoparticle geometry allows straightforward analytical solutions [71]. The experimental situation along with the theoretical model is shown in Fig. 5. For simplicity, we assume that the dipole $\mathbf{p}$ of the molecule is pointing toward the nanoparticle in direction $\mathbf{n}_z$ and that the incident field $\mathbf{E}_o$ is parallel to $\mathbf{p}$. Furthermore, we assume that the intrinsic quantum yield of the molecule is unity, i.e., that the molecule radiates all the power that is supplied to it. The polarizability of the nanoparticle is approximated by its isotropic, quasi-static limit by $\alpha = 4\pi\varepsilon_o a^3[(\varepsilon(\omega)-1)/(\varepsilon(\omega)+2)]$, with $a$ being the particle radius and $\varepsilon$ the particle's relative dielectric permittivity. The resonance condition arising from the denominator of this expression ($\text{Re}\{\varepsilon\}=-2$) is the well-known localized surface plasmon resonance for a sphere [51]. Similar resonance conditions are calculated for nanoparticle antennas with other shapes (e.g., ellipsoids).

Figure 5
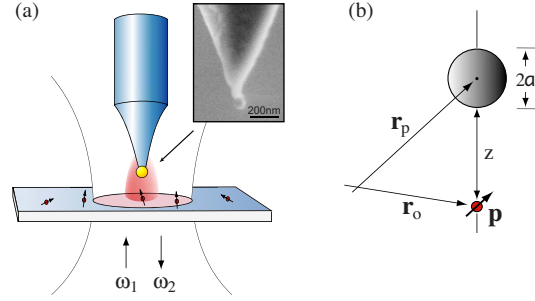


(a) An optical antenna in the form of a gold or silver nanoparticle attached to the end of a pointed glass tip is interacting with a single molecule. The inset shows an scanning electron microscope image of a 80 nm gold particle attached to a glass tip. (b) Theoretical model.

To first order, the field at the molecule's origin due to the incident field $\mathbf{E}_o$ is

$$\mathbf{E} = \left[ \overset{\leftrightarrow}{\mathbf{I}} + \frac{k^2}{\varepsilon_o} \alpha(\omega) \overset{\leftrightarrow}{\mathbf{G}}(\mathbf{r}_o, \mathbf{r}_p, \omega) \right] \mathbf{E}_o = \left[ 1 + 2\tilde{\alpha}(\omega) \frac{a^3}{(a+z)^3} \right] \mathbf{E}_o, \qquad (31)$$

where $k = \omega/c$, $\alpha_p = \tilde{\alpha}_p 4\pi\varepsilon_o a^3$, $\overset{\leftrightarrow}{\mathbf{I}}$ is the unit tensor, and $z$ is the separation between the molecule and the particle's surface. Notice that in the dipole limit $(a \ll \lambda)$ $\tilde{\alpha}_p$ depends only on the shape of the nanoparticle antenna and not on its size. We retain only the near-field term of the free-space Green's function $\overset{\leftrightarrow}{\mathbf{G}}$ and assume that retardation can be neglected. Similarly, the dipole induced in the nanoparticle due to the radiating molecule is

$$\mathbf{p}_p = \frac{k^2}{\varepsilon_o} \alpha_p(\omega) \overset{\leftrightarrow}{\mathbf{G}}(\mathbf{r}_p, \mathbf{r}_o, \omega) \mathbf{p} = 2\tilde{\alpha}_p(\omega) \frac{a^3}{(a+z)^3} \mathbf{p}. \qquad (32)$$

Using Eqs. (31) and (32) we can derive various antenna parameters for the nanoparticle antenna.

**1. Received Power.** According to Eqs. (7), (22), and (31) the normalized total power absorbed by the molecule is

$$\frac{\mathrm{P}_{\mathrm{exc}}}{\mathrm{P}_{\mathrm{exc}}^o} = \frac{\Gamma_{\mathrm{exc}}}{\Gamma_{\mathrm{exc}}^o} = \left| 1 + 2\tilde{\alpha}_p(\omega) \frac{a^3}{(a+z)^3} \right|^2, \qquad (33)$$

where we have used the proportionality between P and $\Gamma$ according to Eq. (10). $\mathrm{P}^o$ and $\Gamma^o$ are calculated in the absence of the nanoparticle antenna.

**2. Radiated Power.** For a particle much smaller than the wavelength of radiation we can neglect the power radiated by higher-order multipoles. Therefore, the total power radiated by the molecule in presence of the antenna is proportional to the absolute square of the total dipole $\mathbf{p} + \mathbf{p}_p$. Using Eq. (32) we find

$$\frac{\mathrm{P}_{\mathrm{rad}}}{\mathrm{P}_{\mathrm{rad}}^o} = \frac{\Gamma_{\mathrm{rad}}}{\Gamma_{\mathrm{rad}}^o} = \frac{|\mathbf{p} + \mathbf{p}_p|^2}{|\mathbf{p}|^2} = \left| 1 + 2\tilde{\alpha}_p(\omega) \frac{a^3}{(a+z)^3} \right|^2, \qquad (34)$$

which is identical to the normalized excitation rate in Eq. (33).

**3. Directivity.** In the absence of the antenna the directivity of the molecule is defined by the dipole radiation pattern $D^o = D^o_\theta = (3/2)\sin^2\theta$. The nanoparticle antenna does not change the directivity because the induced dipole moment $\mathbf{p}_p$ points in the same direction as the molecular dipole, and because the two dipoles are closely spaced. Therefore,

$$D(\theta, \varphi) = D_\theta(\theta, \varphi) = (3/2)\sin^2\theta. \tag{35}$$

Because the directivities $D_\theta$ and $D^o_\theta$ are identical, Eq. (27) implies that the normalized excitation rate is the same as the normalized radiative rate, which also follows from Eqs. (33) and (34). The situation would be more complicated if we considered a dipole $\mathbf{p}$ oriented at an angle to the $z$ axis or an incident wave coming in from a different direction.

**4. Efficiency.** To calculate the radiation efficiency $\varepsilon_{\text{rad}}$ we need to determine the power absorbed in the nanoparticle antenna. For small distances between molecule and particle the curvature of the particle's surface can be neglected and the environment as seen by the molecule is a plane interface [78,32,79]. From electrostatic image theory [51] the normalized absorbed power of a vertical dipole near a half-space with dielectric constant $\varepsilon(\omega)$ is [71]

$$\frac{\text{P}_{\text{loss}}}{\text{P}^o_{\text{rad}}} = \frac{3}{4}\,\text{Im}\left[\frac{\varepsilon(\omega)-1}{\varepsilon(\omega)+1}\right]\frac{1}{(kz)^3}. \tag{36}$$

The resonance of the above expression is worth noting: losses incurred by the radiating dipole correspond to the excitation of surface plasmons along the planar surface given by the familiar condition $\text{Re}\{\varepsilon\} = -1$. Unlike the dipolar localized surface plasmon resonance, this resonance is nonradiative, and the absorbed energy is ultimately lost as heat. Higher-order correction terms to Eq. (36) can be derived as outlined in the literature [32,80]. Combining Eqs. (34) and (36), the radiation efficiency $\varepsilon_{\text{rad}}$ can be calculated for different intrinsic quantum yields $\eta_i$. Figure 6 shows $\varepsilon_{\text{rad}}$ for a molecule with different $\eta_i$ as a function of separation $z$ from a 80 nm gold particle. Evidently, the lower $\eta_i$, the more the antenna increases the overall efficiency, an effect that was observed in 1983 by Wokaun *et al.* [81]. However, the distance between molecule and antenna is very critical. For too large distances there is no interaction between molecule and antenna, and for too small distances all the energy is dissipated into heat. Much higher enhancements of the efficiency can be achieved with optimized antenna designs.

**5. LDOS.** According to Eq. (9) the local density of states is related to the total power P dissipated by a point emitter. Because $\text{P} = \text{P}_{\text{loss}} + \text{P}_{\text{rad}}$ we find

$$\rho_z(z) = \frac{\omega^2}{\pi^2 c^3}\left[\left|1 + 2\left[\frac{\varepsilon(\omega)-1}{\varepsilon(\omega)+2}\right]\frac{a^3}{(a+z)^3}\right|^2 + \frac{3}{4}\,\text{Im}\left[\frac{\varepsilon(\omega)-1}{\varepsilon(\omega)+1}\right]\frac{1}{(kz)^3}\right]. \tag{37}$$

The first term within the brackets denotes the interference between its directly radiated field and the dipole's field scattered by the particle, while the second term corresponds to the power dissipated into heat. The impedance $Z$ follows directly from the LDOS according to Eq. (11).

**6. Aperture.** The intensity incident on the antenna–molecule system is $I = (1/2)\varepsilon_o c|\mathbf{E}_o|^2$. Using the result in Eq. (33) and the expression for the received
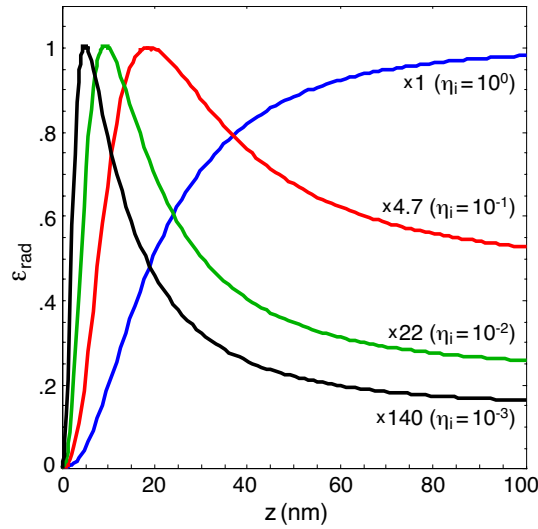
Radiation efficiency $\varepsilon_{rad}$ as a function of separation between a gold nanoparticle antenna and a molecule with different quantum efficiencies $\eta_i$. The lower $\eta_i$ is, the higher the radiation enhancement can be. The curves are scaled to the same maximum value.

power in absence of the antenna, $P^o_{exc} = (\omega/2)\mathrm{Im}\{\alpha\}|\mathbf{E}_o|^2$, we find

$$\sigma = \frac{k}{\varepsilon_o}\,\mathrm{Im}\{\alpha(\omega)\}\left|1 + 2\left[\frac{\varepsilon(\omega)-1}{\varepsilon(\omega)+2}\right]\frac{a^3}{(a+z)^3}\right|^2. \qquad (38)$$

Here, $(k/\varepsilon_o)\mathrm{Im}\{\alpha\}$ corresponds to the molecule's cross section $\sigma_o$ in the absence of the antenna.

The nanoparticle serves as a model antenna, and its predictions have been tested in recent experiments [23,24,71,76,77]. Because the antenna parameters depend on the properties of the environment they can be used as local probes in spectroscopy and microscopy [76].

## 3.7. Wavelength Scaling

Metals at radio frequencies have very large conductivities and are thus almost perfect reflectors. The depth that fields penetrate into them, called the *skin depth*, is negligible compared with any relevant length scale of the antenna. However, at optical frequencies electrons in metals have considerable inertia and cannot respond instantaneously. The skin depth is consequently of the order of tens of nanometers, comparable with the dimensions of the antenna. Traditional design rules that prescribe antenna parameters only in terms of an external wavelength are thus no longer valid. Rigorously treating the metal as a strongly coupled plasma is required, which leads to a reduced effective wavelength seen by the antenna [82]. This effective wavelength $\lambda_{eff}$ is related to the external (incident) wavelength $\lambda$ by the surprisingly simple relation

$$\lambda_{\text{eff}} = n_1 + n_2 \left[ \frac{\lambda}{\lambda_p} \right], \tag{39}$$

where $\lambda_p$ is the plasma wavelength of the metal and $n_1$ and $n_2$ are constants that depend on the geometry and dielectric parameters of the antenna. $\lambda_{\text{eff}}$ is roughly a factor of 2–6 shorter than the free space $\lambda$ for typical metals (gold, silver, aluminum) and realistic antenna thicknesses [82,83].

The notion of an effective wavelength can be used to extend familiar design ideas and rules into the optical frequency regime. For example, the optical analog of the $\lambda/2$ dipole antenna becomes a thin metal rod of length $\lambda_{\text{eff}}/2$. Since $\lambda_{\text{eff}}$ for a gold rod of radius 5 nm is roughly $\lambda/5.3$ [see Fig. 7(c)], this means that the length of a $\lambda/2$ dipole antenna is surprisingly small, about $\lambda/10.6$. One can similarly construct antenna arrays like the well-established Yagi–Uda antenna developed in the 1920s for the UHF–VHF region [67,82].

Figure 7(a) shows the intensity distribution near a half-wave antenna of length $L=110$ nm and radius $R=5$ nm resonantly excited at $\lambda=1170$ nm. The effective wavelength is $\lambda_{\text{eff}}=220$ nm. The induced current density $\mathbf{j}=-i\omega\varepsilon_o[\varepsilon(\omega)-1]\mathbf{E}$ evaluated along the axis of the antenna is shown in Fig. 7(a). The current density can be accurately approximated by $j \propto \cos[z\pi/(L+2R)]$. The current is nearly 180° out of phase with respect to the exciting field.

The wavelength shortening from $\lambda$ to $\lambda_{\text{eff}}$ has interesting implications. For example, it implies that the radiation resistance of an optical half-wave antenna is of the order of just a few ohms [82,84,85]. To see this, we note that the radiation resistance of a thin-wire antenna is roughly $R_{\text{rad}}=30\pi^2(L/\lambda)^2$, with $L$ being the antenna length. For a half-wave antenna at RFs $L=\lambda/2$ and $R_{\text{rad}} \sim 73$ Ω.

## Figure 7
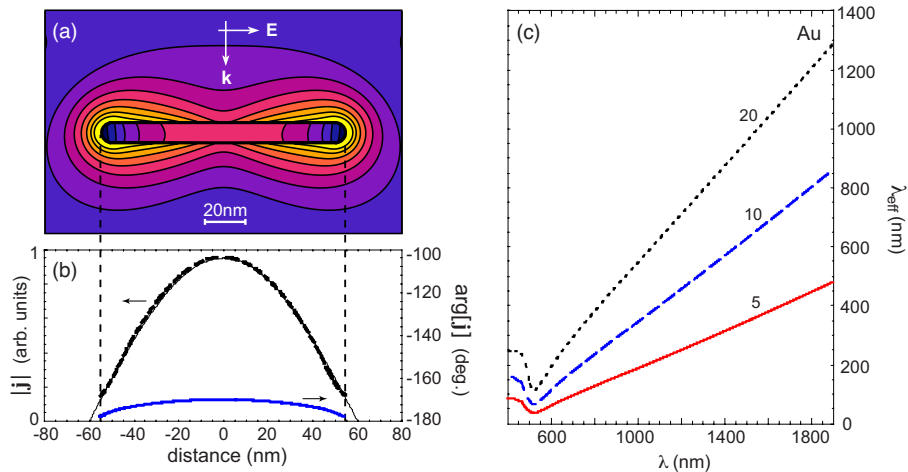


Effective wavelength scaling for linear gold antennas. (a) Intensity distribution ($E^2$, factor of 2 between contour lines) for a gold half-wave antenna irradiated with a plane wave ($\lambda=1150$ nm). (b) Amplitude and phase of the current density ($\mathbf{j}$) evaluated along the axis of the antenna. (c) Effective wavelength scaling for gold rods of different radii (5, 10, and 20 nm).

However, for an optical half-wave antenna, $L=\lambda_{\mathrm{eff}}/2$ , and hence $R_{\mathrm{rad}}$ $=(30/4)\pi^2(\lambda_{\mathrm{eff}}/\lambda)^2$. In other words, the radiation resistance at optical frequencies is a factor of $(\lambda_{\mathrm{eff}}/\lambda)^2$ smaller than at RFs. For $\lambda_{\mathrm{eff}}=\lambda/5$ we find $R_{\mathrm{rad}}=3\ \Omega$.

Interestingly, while the radiation resistance $R_{\mathrm{rad}}$ at optical frequencies is a factor $(\lambda_{\mathrm{eff}}/\lambda)^2$ smaller than at RFs, the loss resistance $R_{\mathrm{loss}}$ is only a factor $(\lambda_{\mathrm{eff}}/\lambda)$ smaller. This follows from $\mathrm{P}_{\mathrm{loss}}=VI=R_{\mathrm{loss}}I^2$, with $V=E/L$ and $I\propto\omega\varepsilon_o\ \mathrm{Im}\{\varepsilon\}E$. Using $L=\lambda_{\mathrm{eff}}/2$ we obtain $R_{\mathrm{loss}}\propto\lambda\lambda_{\mathrm{eff}}/\mathrm{Im}\{\varepsilon\}$. At RFs $\lambda_{\mathrm{eff}}=\lambda$, and therefore the loss resistance is a factor $(\lambda_{\mathrm{eff}}/\lambda)$ smaller at optical frequencies than at RFs. For metals with no loss $(\mathrm{Im}\{\varepsilon\}\rightarrow 0)$ the resistance tends to infinity, implying that no current can flow for a given field $E$.

## 3.8. Influencing the Light–Matter Interaction

In the discussion so far we have assumed that the antenna does not influence the intrinsic properties of the emitter or transmitter. Modifications of the transition rates occurred because of a change in the LDOS and not because of a change in molecular polarizability $\alpha$. However, the highly localized fields near the antenna open up new interaction mechanisms between light and matter, such as higher-order multipole transitions or momentum-forbidden transitions. These interactions are inaccessible in free space and have the potential to enrich optical spectroscopy and provide new strategies for optical sensing and detection.

In free space, the momentum of a photon with energy $E=\hbar\omega$ is $p_{\mathrm{ph}}=\hbar\omega/c$. On the other hand, the momentum of an unbound electron with the same energy is $p_e=[2m^*\hbar\omega]^{1/2}$, which is a factor of $[2m^*c^2/(\hbar\omega)]^{1/2}\approx 10^2\dots 10^3$ larger than the photon momentum. Therefore, the photon momentum can be neglected in electronic transitions; i.e., optically excited transitions are vertical in an electronic band diagram. However, near optical antennas the photon momentum is no longer defined by its free space value. Instead, the localized optical fields are associated with a broad momentum distribution whose bandwidth $p_{\mathrm{ph}}=\pi\hbar/\Delta$ is given by the spatial confinement $\Delta$, which can be as small as $1-10$ nm. Thus, in the optical near field the photon momentum can be increased by a factor of $\lambda/\Delta\sim 100$, which brings it into the range of the electron momentum, especially in materials with small effective mass $m^*$. Hence, localized optical fields can give rise to diagonal transitions in an electronic band diagram, thereby increasing the overall absorption strength represented by $\mathrm{Im}\{\alpha\}$, which is useful for devices such as silicon solar cells (see Subsection 4.2). The increase of photon momentum in optical near fields has been discussed in the context of photoelectron emission [86] and photoluminescence (PL)[87].

The strong field confinement near optical antennas also has implications for selection rules in atomic or molecular systems. The light–matter interaction involves matrix elements of the form $\langle f|\hat{\mathbf{p}}\cdot\hat{\mathbf{A}}|i\rangle$, with $\hat{\mathbf{p}}$ and $\hat{\mathbf{A}}$ being the momentum and the field operators, respectively. As long as the quantum wave functions of states $|i\rangle$ and $|f\rangle$ are much smaller than the spatial extent over which $\hat{\mathbf{A}}$ varies, it is legitimate to pull $\hat{\mathbf{A}}$ out of the matrix element. The remaining expression $\langle f|\hat{\mathbf{p}}|i\rangle$ is what defines the dipole approximation and leads to standard dipole selection rules. However, the localized fields near optical antennas give rise to spatial variations of $\hat{\mathbf{A}}$ of a few nanometers, and hence it may no longer be legitimate to invoke the dipole approximation. This is especially the case in semiconductor nanostructures where the low effective mass gives rise to quantum orbitals with

large spatial extent. In situations where the field confinement becomes comparable with quantum confinement it is possible to expand the light–matter interaction in a multipole series. Theoretical studies have shown that higher-order multipoles have different selection rules [88,89]. Additional transition channels are opened up in near-field interactions, which can be exploited for boosting the sensitivity of photodetection. Once the field confinement becomes stronger than the quantum confinement the multipole series no longer converges, and transition rates are solely defined by the local overlap of ground state and excited state wave functions. In this limit, an optical antenna can be used to spatially map out the quantum wave functions, providing direct optical images of atomic orbitals. However, this would require antennas with field confinements of better than 1 nm.

## 3.9. Nonlinear Antenna Behavior

Today, most optical antenna designs are based on the optical properties of metals. In the linear regime the behavior is well described by a free electron gas. Additional interband transitions give rise to the characteristic color of a metal. Nonlocal effects come into play when the size of the structures becomes comparable with the electron mean free path [90–93], such as close to corners, tips, and gaps. Interestingly, metals also have a very strong nonlinear response. For example, the third-order nonlinear susceptibility of gold ($\chi^{(3)} \sim 1$ nm$^2$/V$^2$) is more than 3 orders of magnitude larger than the susceptibility of the most nonlinear optical crystals, such as lithium niobate (LiNbO$_3$) [94–96]. Laser systems employ nonlinear crystals instead of noble metals for frequency conversion because they are transparent, enabling them to be placed in a beam line, and because they allow phase matching—the coherent addition of the nonlinear response on propagation through a periodic crystal. For phase matching to occur the crystal needs to be many wavelengths in size. In plasmonics, one is usually more concerned with local nonlinear signals, and without the constraints associated with lasers, exploiting the nonlinearities of noble metal antenna structures may be favorable. Nonlinear plasmonics is a largely unexplored territory and only a few nonlinear interactions in noble metal nanostructures have been studied so far, including second-harmonic generation [97,98], third-harmonic generation [99], two-photon excited luminescence (TPL) [87,100–102], and four-wave mixing [103,104]. Figure 8 shows the spectrum of photons emitted from a pair of gold nanoparticles in touching contact irradiated with laser pulses of wavelength $\lambda_1$ =810 nm and $\lambda_2$=1210 nm. The discrete peaks correspond to coherent nonlinear processes, whereas the broad continuum is associated with TPL. The intensity drop toward the red ($\lambda_{em} > 570$ nm) is due to the optical filters used to suppress the excitation lasers.

The high optical nonlinearities of metals bring many opportunities for nanoscale photonic devices. For example, the intensity of optical four-wave mixing in a gold nanoparticle junction spans 4 orders of magnitude with a gap variation of only 2 nm [103] (see Fig. 9). Optical four-wave mixing uses two incident laser beams with frequencies $\omega_1$ and $\omega_2$ to produce radiation at frequency $\omega_{4WM}$ $=2\omega_1-\omega_2$. Figure 9(b) demonstrates that a pair of gold nanoparticles can be used as a spatially and temporally controllable photon source. The ability to generate local frequency conversion with high efficiency makes it possible to exploit frequency-selective interactions across the entire visible and IR spectrum while requiring only a single frequency excitation. Frequency-converted fields
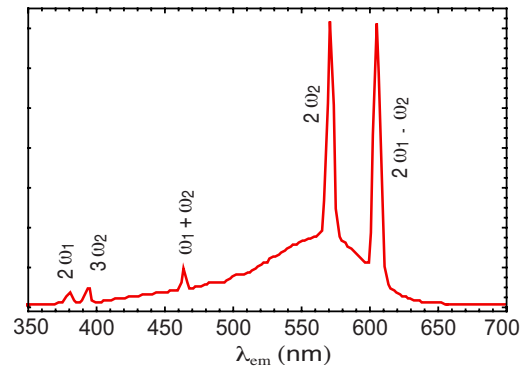
Spectrum of photons emitted from a pair of gold nanoparticles irradiated with laser pulses of wavelength $\lambda_1 = 810$ nm and $\lambda_2 = 1210$ nm. Each peak is associated with a different nonlinear process. From [105].

Figure 9
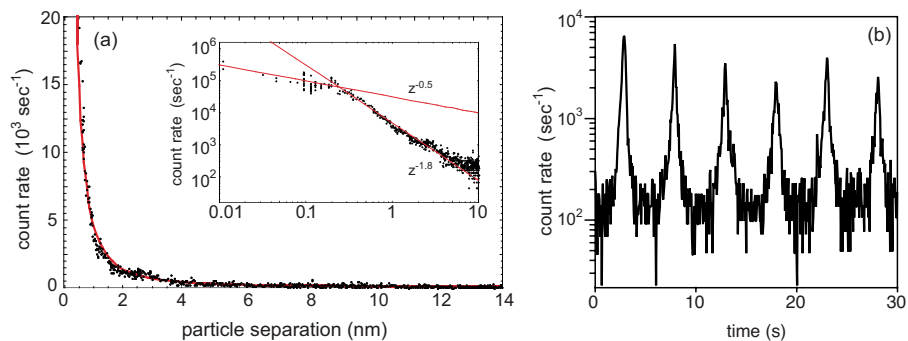


(a) Four-wave mixing photon count rate ($\lambda_{4WM} = 639$ nm) as a function of the separation of two 60 nm gold nanoparticles. Inset, detailed view on a log-log scale. Dots are data, and the curves are power-law fits. The kink in the curve indicates the formation of a conductive bridge. (b) Photon bursts generated by modulating the interparticle separation. Reprinted with permission from [103]. © 2007 American Physical Society.

can be used to interact with nanoscale systems like single quantum dots, molecules, or ions. The challenge for optical antenna design is that the structures need to be resonant simultaneously at multiple wavelengths—the wavelengths of incoming radiation and the wavelengths of outgoing radiation. Nonlinear optical antennas hold promise for frequency conversion on a single-photon level and for single-photon transistors [106]: devices that employ the energy of a single photon to switch between states.

## 3.10. Characterization of Optical Antennas

The nanoscale dimensions of optical antennas bring with them associated characterization challenges. Resonant light scattering is a popular technique both theoretically and experimentally for studying size- and shape-related optical

resonances in antenna structures [107–111]. Linear antenna structures, such as nanorods or nanostrips, are strongly analogous to Fabry–Perot resonators [112–114] and can support higher-order resonances in addition to the fundamental dipole mode [115,116]. A direct visualization of field distributions around antennas using near-field scanning microscopy has been demonstrated in the mid-IR for micrometer-sized structures [117,118], but the absence of ultrasmall probes capable of resolving details of the order of a nanometer currently impedes the extension of this technique to antennas for the visible. The only technique that currently approaches such level of detail is electron energy loss spectroscopy, which utilizes a tightly focused electron beam to probe the LDOS directly. This nonoptical technique has been used to map energy-resolved plasmon eigenmodes on single nanoparticles [119,120].

An alternative characterization modality uses the nonlinear responses of antennas mentioned in Subsection 3.9. TPL is a second-order process especially suited for mapping out intensity hot spots in antennas generating a high degree of field localization, such as the bowtie [121,122], half-wave [102], or gap antennas [123,102]. Figure 10 shows field intensities in antenna test structures revealed by far-field TPL measurements using femtosecond laser excitation. As expected, the strongest enhancements arise in the gap region when the incoming light is polarized along the length of the antenna. To increase the spatial resolution in TPL imaging, Bouhelier *et al.* employed a sharp tip to locally scatter the TPL signal generated by the antenna under study [100]. The tip is raster scanned over the laser-irradiated antenna in close proximity, and the TPL intensity is measured as a function of the tip's scan coordinates. In order not to perturb the antenna's behavior, care must be taken to avoid any strong interaction between the local scatterer and the antenna under study.

As an aside, one must note the difference in the role of the feed gap between the radio and optical regimes. The feed gap in a radio antenna is typically impedance matched to a generator (source) and is **not** a point of high localized energy density. This matching ensures that the two antenna segments do not feel a gap or discontinuity between them. The gap in an optical gap antenna, in contrast, is a

## Figure 10
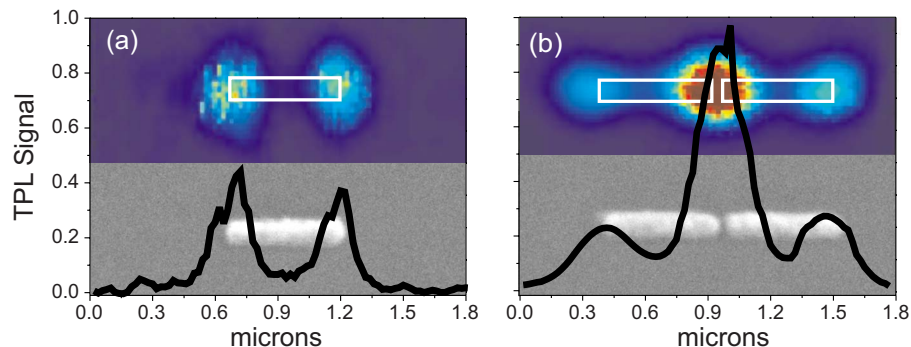
Two-photon excited luminescence as a tool to characterize field intensity distributions in optical antennas. (a) Resonantly excited linear nanostrip antenna showing field enhancement at the ends. (b) TPL from a gap antenna, indicating a strong field enhancement in the gap for incoming light polarized along the long axis. Reprinted with permission from [102]. © 2008 American Physical Society.

region of high local field intensity and dictates the antenna's overall optical response. It is a high impedance point due to the large LDOS (see Subsection 3.2), and the efforts over the years to engineer the gap for strongest field enhancement are a direct consequence. The mismatched gap can even be turned into an advantage as it provides a means to tune antenna properties, e.g., by loading the gap with various nanoloads [85,124,125]. Such a tuning may enable one to go beyond simple field enhancement and might lead to truly impedance-matched energy transfer between a localized source and the antenna.

# 4. Applications of Optical Antennas

Research in the field of optical antennas is currently driven by the need for high field enhancement, strong field localization, and large absorption cross sections. This includes antennas for high-resolution microscopy and spectroscopy, photovoltaics, light emission, and coherent control. In one way or another, optical antennas are used to make processes more efficient or to increase the specificity of gathered information. In this section, we review recent advances, highlight application areas, and discuss future developments in the field of optical antennas.

## 4.1. Antennas for Nanoscale Imaging and Spectroscopy

The hallmark of optical antennas, their ability to influence light on the nanometer scale, leads naturally to nanoimaging applications. In the context of nanoscale imaging, an optical antenna represents a near-field optical probe used to interact locally with an unknown sample surface. To acquire a near-field optical image, the optical antenna is guided over the sample surface in close proximity and an optical response (scattering, fluorescence, antenna detuning) is detected for each image pixel. In general, a near-field image recorded in this way renders the spatial distribution of the antenna–sample interaction strength, and **not** the properties of the sample. It is possible, however, to write the interaction between antenna and sample as a series of interaction orders [126], and in many cases it is legitimate to retain only a single dominant term. For example, in scattering-based near-field microscopy, the antenna acts as a local perturbation that scatters away the field near the sample surface. Therefore, the antenna–sample interaction can be largely neglected. At the other extreme, in tip-enhanced near-field optical microscopy, the sample interacts predominantly with the locally enhanced antenna field, and the external irradiation can be largely ignored. In this regime the optical antenna acts as a nanoscale flashlight [127] that can be used to perform local spectroscopy.

There is a considerable body of literature on microscopy and spectroscopy aided by antennas, which has been covered in several recent reviews [59,51,82,128–131]. Our goal below is not to provide a comprehensive review of the field, but rather to convey the basic concepts with some examples.

### 4.1a. Scattering-Based Microscopy

The optical field near an irradiated sample consists of both propagating and evanescent field components. The inability of the imaging apparatus to collect the evanescent fields results in the resolution limit. The basic idea behind scattering based near-field microscopy is to locally convert the evanescent fields into

propagating radiation by use of a scattering probe. The first experiments performed in the early 1990s used sharp metal tips [132,133], although semiconducting atomic force microscopy tips have since become the prevalent choice. Samples that couple strongly with the illuminating laser radiation (e.g., due to plasmon or phonon resonances) are best suited for scattering microscopy studies. As a consequence, most studies to date have investigated metallic nanostructures excited in the visible or near-IR [134,135] and semiconductors in the mid-IR [136]. Driven by the need for efficient signal extraction from a large background, Knoll and Keilmann proposed modulating the tip vertically (at frequency $\Omega$) and demodulating the signal at higher harmonics ($n\Omega$) [137]. This technique was later combined with a heterodyne scheme to extract optical amplitude and phase information of the scattered light [138,139].

In most scattering-based approaches it is assumed that the incident light interacts more strongly with the sample surface than with the local probe. Therefore, the resulting images reflect primarily the properties of the sample. However, the sample properties always act back on the local probe and influence its properties. This back-action has been recently studied in an elegant experiment by Sandoghdar and co-workers using a local probe in the form of a single gold nanoparticle [76]. The properties of this nanoparticle antenna, such as its resonance frequency and scattering strength, were found to be dependent on the local environment defined by the sample properties. Therefore, the antenna detuning becomes a local probe for the properties of the sample. An example of these studies is shown in Fig. 11, which renders a spatial map of the width of the antenna resonance recorded while scanning the nanoparticle antenna over a test structure. The nanoparticle antenna has also been recently used by Eng and co-workers to demonstrate scattering microscopy in the mid-IR using an 80 nm gold nanoparticle [140].

### 4.1b. Spectroscopy Based on Local Field Enhancement

An effective antenna interacts strongly with incoming radiation and leads to a high degree of field localization. The localized fields have been used in several

**Figure 11**
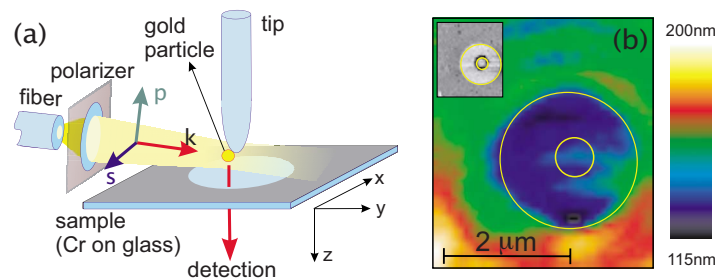
Microscopy using environment-induced spectral changes of an optical antenna. (a) Schematic of the experiment. A white light source illuminates a 100 nm gold nanoparticle antenna from the side. (b) A spatial map of the width of the antenna's plasmon resonance recorded by raster scanning the nanoparticle antenna over a sample consisting of a circular hole in a layer of 8 nm thick chromium (see inset). Adapted with permission from [76]. © 2005 American Physical Society.

recent experiments as excitation sources for local spectroscopy, such as fluorescence, IR absorption, and Raman scattering.

Laser-excited fluorescence is a widely used analytical tool because fluorescence can be significantly redshifted from excitation (Stokes shift), rendering the signal essentially background free. Even though fluorescence does not typically reveal molecular information, and neither are fluorescent dyes particularly long-lived (photobleaching), it offers single-molecule sensitivity even without any antennas [141] because of the large absorption cross sections of fluorescent dyes $(\sim 10^{-15}$ cm$^2$). The fluorescence rate $\Gamma_{fl}$ from a single emitter is determined by the excitation rate $\Gamma_{exc}$ and the intrinsic quantum yield $\eta_i$ of the emitter. $\eta_i$ is defined analogously to Eq. (13) as $\Gamma_{rad}^o/(\Gamma_{rad}^o + \Gamma_{nr}^o)$, where $\Gamma_{rad}^o$ and $\Gamma_{nr}^o$ are the intrinsic radiative and nonradiative relaxation rates, respectively. In the absence of the antenna and far from saturation (weak excitation) the fluorescence rate is given by

$$\Gamma_{fl} = \Gamma_{exc}^o \cdot \eta_i = \Gamma_{exc} \frac{\Gamma_{rad}^o}{\Gamma_{rad}^o + \Gamma_{nr}^o}. \tag{40}$$

The antenna typically leads to an increase in $\Gamma_{exc}$ due to local field enhancement and the associated increase of the LDOS. By reciprocity [cf. Eq. (27)], an increase in $\Gamma_{exc}$ is accompanied by an increase of $\Gamma_{rad}$ [24,53,142,143]. However, the presence of the antenna also increases $\Gamma_{nr}$ because of nonradiative energy transfer from the excited molecule to the antenna [144–146]. Good emitters have $\eta_i \approx 1$, which cannot be further increased by an optical antenna. Therefore, an antenna-induced increase in fluorescence is basically a result of an increase in $\Gamma_{exc}$. On the other hand, for poor emitters with $\eta_i \ll 1$ (i.e., $\Gamma_{nr}^o \gg \Gamma_{rad}^o$), the antenna can end up enhancing both the excitation rate and the efficiency (see Fig. 6), leading to much higher net fluorescence enhancements than those for good emitters [81,147].

Hartschuh *et al.* studied PL from single-walled carbon nanotubes and reported PL enhancements of around 100, using sharp gold tips [148–150] (Fig. 12). Such high enhancements are consistent with the low intrinsic PL quantum yield of $\sim 10^{-3}$ experimentally observed for single-walled carbon nanotubes, which is a result of large intrinsic $\Gamma_{nr}$ [151]. Tam *et al.* used single silica-gold core-shell particles (nanoshells) for plasmonic fluorescence enhancement of adsorbed molecules with low $\eta_i$ in the near-IR [152]. Silicon quantum dots, which also have a low intrinsic quantum yield, have been studied by the groups of Atwater and Polman, and the luminescence was shown to increase close to patterned silver islands [153,154].

The key to having efficient antennas for fluorescence enhancement is to minimize nonradiative losses in the metal (quenching). Extended structures, such as sharp metal tips, allow relaxation of an excited emitter into propagating surface plasmons along the tip and therefore lead to high losses [155]. Confined nanostructures such as noble metal nanoparticles strike a balance between strong field enhancement and low absorption and are thus ideal for fluorescence applications. Enhancements of up to 20 have been reported by using gold and silver nanoparticles on single fluorophores [24,23,77]. Spectral dependence of $\Gamma_{exc}$ and $\Gamma_{nr}$ has been investigated to clarify the role of surface plasmon resonance in nanoparticle antennas [71,156,157]. Biological moieties with sizes comparable with the size of the antenna are of particular interest in fluorescence imaging
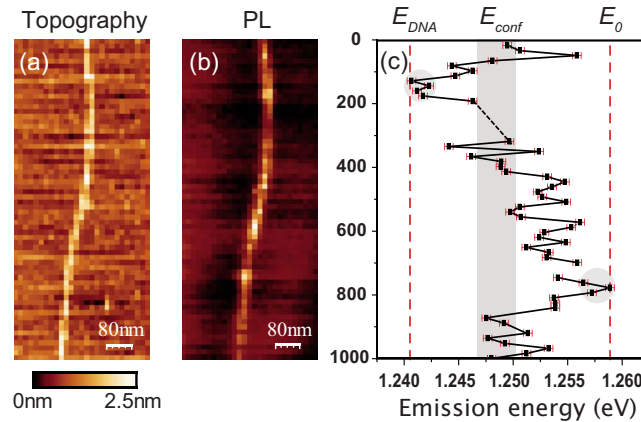
PL from carbon nanotubes enhanced with gold tips. (a) Sample topography consisting of a DNA-wrapped nanotube on mica. (b) Corresponding PL image formed by integrating the signal from 850 to 1050 nm (laser excitation is at 633 nm). (c) Variations of the peak emission frequency due to DNA wrapping. Reprinted with permission from [150]. © 2008 American Chemical Society.

[158], and single proteins have recently been visualized in physiological conditions by using a single gold nanoparticle [159,160].

A top-down alternative to using colloidal nanoparticles is to fabricate a grounded monopole antenna by focused ion-beam milling on top of a small nanometric aperture [61] (see Fig. 13) This approach has the advantage of reducing the background confocal excitation that plagues other techniques. A closely re-

Figure 13
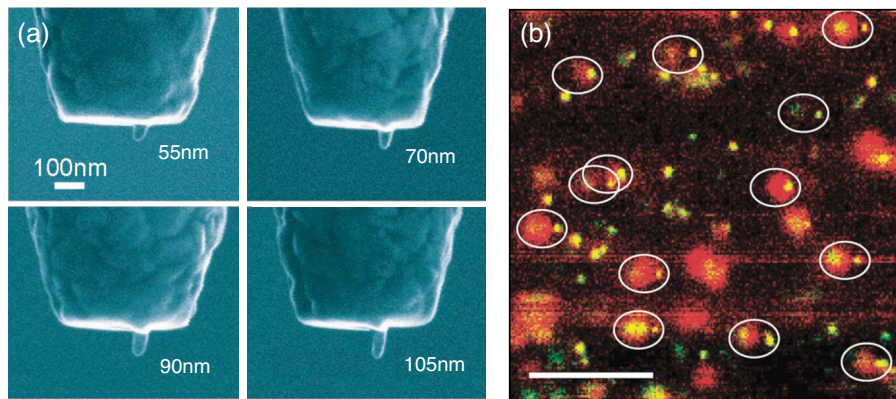


Single-molecule fluorescence imaging using a $\lambda/4$ monopole antenna fabricated on the end face of an aperture-type near-field probe. (a) Electron micrographs showing monopoles of different lengths, resonant at correspondingly different wavelengths. From [61]. (b) Spatial fluorescence map of randomly oriented single molecules. The emitted polarization is color coded: red, horizontal; green, vertical; yellow, unpolarized. Scale bar, 1 $\mu$m. Adapted from [62] by permission from Macmillan Publishers Ltd., *Nature Photonics*, © 2008.
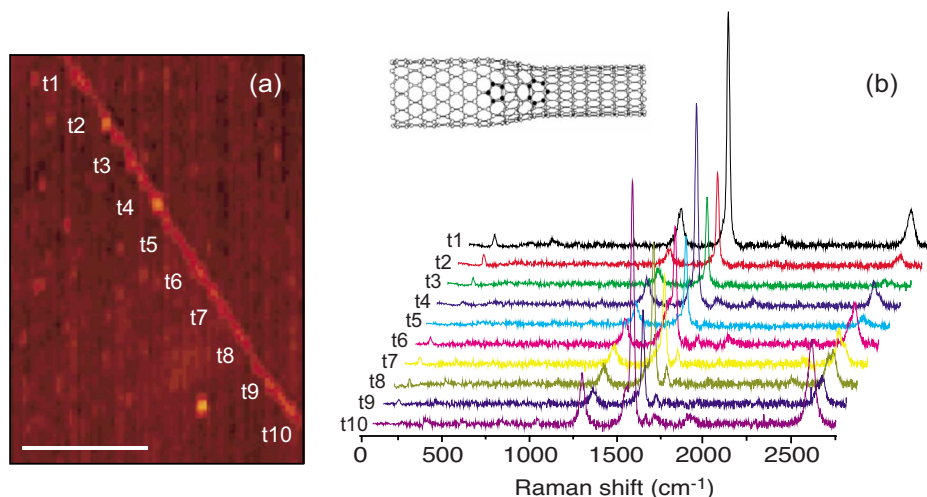
Tip-enhanced Raman spectroscopy of a single-walled carbon nanotube. (a) To-pographic image. The scale bar denotes 200 nm. (b) Near-field Raman spectra recorded at the locations marked in (a). The radial breathing mode frequency changes from 251 to 191 cm$^{-1}$, revealing a structural transition (inset) from a semiconducting (10, 3) tube to a metallic (12, 6) tube. Reprinted with permission from [172]. © 2007 American Chemical Society.

lated technique pioneered by Guckenberger and collaborators makes use of a sharp metal tip grown on an aperture to give a so-called tip-on-aperture probe [161]. Using a tip-on-aperture probe, these researchers demonstrated a spatial resolution of 10 nm while imaging dye-labeled DNA strands [162].

In contrast to fluorescence, the vibrational spectra provided by Raman scattering define a unique chemical fingerprint for the material under study. However, Ra-man scattering cross sections are 10–15 orders of magnitude smaller than typical fluorescence cross sections of dye molecules. Therefore, the effect is generally too weak to detect, and to achieve single molecule sensitivity it is necessary to invoke enhancement mechanisms such as resonance enhancement or field en-hancement. Raman scattering involves the absorption and emission of photons almost identical in energy, and a nearby antenna can amplify both the incoming field and the outgoing field. The total Raman scattering enhancement is there-fore proportional to the fourth power of the field enhancement [163]. Recent studies of SERS revealed that junctions in colloidal nanoparticle clusters can have extremely high field enhancements ($\gtrsim 10^3$), leading to Raman enhance-ments as high as $10^{14}$, sufficient even to detect a single molecule [164–166]. In addition to field enhancement, a chemical contribution to SERS is well known [167], and well-characterized antennas can be useful in separating chemical and electromagnetic contributions in the Raman enhancement mechanism [168].

Although nanoparticle aggregates offer the highest field enhancements, getting the molecules controllably and reproducibly into the hot spot regions is a major challenge. A more flexible and controlled, albeit less efficient, approach is to use optical antennas such as metal tips for point-by-point Raman spectroscopy, simi-lar to the original idea of Wessel [22]. This technique is commonly referred to as tip-enhanced Raman scattering (TERS) [129,169,170]. Raman enhancements

achieved with tips are typically in the range of $10^4 - 10^8$, corresponding to field enhancements of 10–100. Hartschuh, Anderson and co-workers have used TERS to extensively study structural and electronic properties of carbon nanotubes [171,172]. As an example, Fig. 14 shows an intramolecular junction in a carbon nanotube revealed by TERS. Deckert and co-workers applied TERS to the study of biologically relevant samples such as DNA components and bacteria [173,174]. Very recently, Steidtner and Pettinger have shown evidence for single-molecule detection using a combination of TERS and scanning tunneling microscopy [175], furthering previous work done in the groups of Raschke [176] and Zenobi [177].
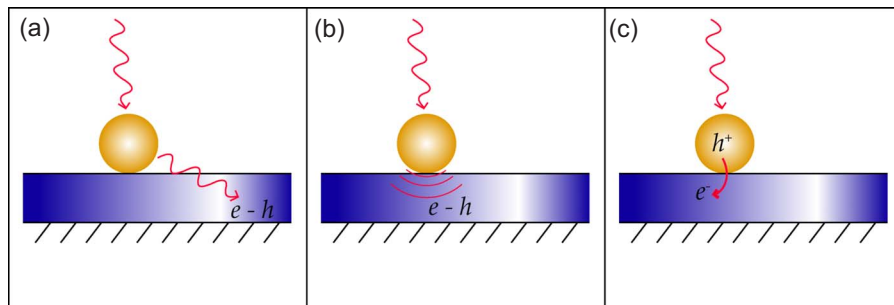
## 4.2. Antennas for Photovoltaics

An RF or microwave receiver antenna typically generates an alternating current in a transmission line. It is straightforward to rectify this current and produce a direct current output. In fact, the basic self-powered crystal radio receiver is based on this idea. The name *rectennas*, short for "rectifying antennas," was coined in the 1960s when a project sponsored by the Department of Defense led to the development of a helicopter whose rotor was powered by onboard rectification of outside microwave radiation [178]. The first suggestion to use rectennas for harvesting solar energy came from Bailey in 1972 [179], and Marks subsequently filed several patents describing possible implementations of optical antenna arrays coupled to metal-insulator-metal rectifying diodes [180–182]. While conversion efficiencies greater than 50% have been achieved at 10 GHz, even a proof-of-principle demonstration of single-digit efficiencies in the IR or visible regime remains a formidable task [183]. This is primarily because of challenges associated with reliable nanofabrication of antenna arrays coupled to ultrafast diodes capable of optical frequency rectification, and not due to any fundamental physical limitations. It is conceivable that inexpensive and efficient solar rectennas will become a reality in the future by using bottom-up approaches combined with greater control over materials processing, or by employing novel materials such as carbon nanotubes [84,184].

The traditional approach to photovoltaics is to use light for generating charge carriers in a semiconductor. The spatial separation of the charge carriers defines a current in an external circuit. For maximum efficiency it is important to absorb most of the incoming radiation, necessitating a minimum material thickness, which forms the primary cost determinant. There are at least three distinct ways in which nanoparticle antennas can interact with a photoactive substrate when placed in close proximity to it, as illustrated in Fig. 15. Plasmonic nanoparticles have large optical cross sections and can efficiently collect and scatter photons into the far field, some of which may become coupled into in-plane waveguide modes in the photoactive material [186,187]. This leads first to an increased effective optical path length and greater photon absorption probability. Second, the spatially localized high-momentum near-field photons created in the immediate vicinity of an optical antenna can directly excite electron–hole pairs in an indirect gap semiconductor (like silicon) even without phonon assistance [188], thereby increasing light absorption per unit thickness. Last, there is the possibility of direct charge-carrier injection from the nanoparticle into the semiconductor.

Making use of the first two effects, Stuart and Hall were the first to show increased absorption using metal nanoparticles in a 165 nm thick silicon-on-

Schematic of different types of antenna effects in photovoltaics. (a) Far-field scattering, leading to a prolonged optical path. (b) Near-field scattering, causing locally increased absorption, and (c) direct injection of photoexcited carriers into the semiconductor. From [185].

insulator material [186]. More recently, Pillai *et al.* demonstrated 16-fold absorption enhancement at $\lambda = 1050$ nm by depositing $>100$ nm silver particles on thin film silicon-on-insulator cells [189], while Atwater and co-workers also saw an improvement in the performance of GaAs thin film solar cells by decorating them with silver nanoparticles [190]. Lim *et al.* explored the effect of spherical gold nanoparticles on optically thick silicon and found a positive effect most likely due to increased waveguiding [191]. Hägglund *et al.* investigated thick silicon further by using gold nanodisks and highlighted the problem of increased losses at the plasmon resonance wavelength, which can more than compensate for an increase of absorption in silicon [192]. Improvements in the performance of organic solar cells [193,194] and InP/InGasAsP quantum-well solar cells [195] have also been reported recently. In all of these examples, the inclusion of nanoparticles in the solar cell structure leads to a reduction in the absorption-mandated thickness requirement for the photoconductive material. A reduced thickness is favorable, especially for organic semiconductors, since it allows a higher fraction of photogenerated carriers to reach the outer world (electrodes) without being lost to undesirable recombination events. A good review of recent developments is given by Catchpole and Polman [196].

Another attractive class of photovoltaic cells is the dye-sensitized solar cell or Grätzel cell [197]. These cells employ extremely fast charge injection from a dye into the conduction band of a large bandgap semiconductor, typically $TiO_2$, instead of the usual approach of generating electron–hole pairs in the semiconductor directly. Early attempts at incorporating metal nanostructures in Grätzel cells gave mixed results [198,199]. Hägglund *et al.* [200] systematically explored this issue by sensitizing a model dye-sensitized solar cell system of flat $TiO_2$ film with nanofabricated gold ellipsoids, as shown in Fig. 16. They found evidence for plasmonically enhanced charge generation rate from the dye, which was attributed to a combination of near-field and far-field effects [200]. Adopting a different approach and improving on initial experiments by Kozuka *et al.* [201], Tian and Tatsuma have replaced the dye completely by gold nanoparticles and made use of direct photocarrier injection from the nanoparticles into $TiO_2$ to get photon-to-current conversion efficiencies as high as 20% [202]. A scenario combining the two effects of direct charge injection and absorption enhancement of the dye in a nanoparticle-enriched Grätzel cell should be easily realizable.

Figure 16
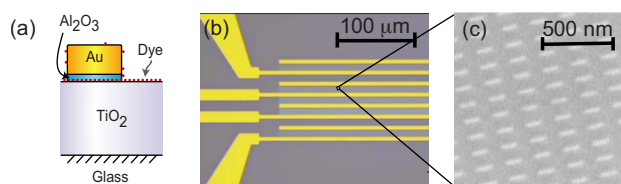


A dye-sensitized solar cell decorated with gold nanodisk antennas for improved absorption of light. (a) Schematic of the device. Excitation of the dye molecules adsorbed on $TiO_2$ is amplified near an antenna, leading to enhanced carrier injection from the dyes into the $TiO_2$. (b), (c) Electron micrographs showing electrical contacts and gold nanodisks fabricated on top of thin $TiO_2$. Reprinted with permission from [200]. © 2008 American Institute of Physics.

## 4.3. Antennas for Light Emission

Because of reciprocity, optical antennas increase not only the efficiency of light absorption but also the efficiency of light emission. They stand to improve inherently low-efficiency lighting schemes like organic LEDs (OLEDs), silicon-based lighting, and solid-state lighting in the yellow and green spectral region.

Typically, an OLED comprises an active organic semiconductor sandwiched between two electrodes. The charges injected from the electrodes recombine as electron–hole pairs (excitons) and then transfer their energy to light-emitting dopants. Despite the simplicity of the system, OLED technology faces several challenges, and optical antenna structures might provide solutions for some of them. Nominally one quarter of excitons are formed in a singlet (spin-zero) state, and three quarters are in a triplet (spin-one) state. However, in most cases the light-emitting dopants can only convert the energy of singlet states into photons, and the energy associated with triplet states is dissipated as heat. The triplet states not only reduce the efficiency but are also believed to reduce the longevity of a device. Optical antennas have the potential to quench the triplet state lifetimes, thereby increasing the long-term stability of OLEDs. Another limitation in OLEDs is that some of the energy released in the recombination process becomes trapped in the conducting electrodes as surface plasmons and is eventually dissipated into heat. By patterning the electrodes with arrays of holes, this energy can be released from surface plasmon modes and emitted into free space [203–205]. Liu *et al.* show a factor-seven improvement in the electroluminescence quantum efficiency of an OLED device [204]. They attribute this phenomenon to the enhanced transmission of the electroluminescence through the perforated electrode. Perforations in such a metal act as antennas, allowing plasmon modes to couple to propagating radiation.

A similar effect can be achieved by using metallic particles instead of holes and has found success in the field of silicon lighting. Philip Ball's 2001 review of the state of silicon light emission lists quantum dots and texture engineering as ways to increase the emission efficiency, but makes no mention of the use of antennas or metallic nanoparticles [206]. Two years earlier, W. L. Barnes had suggested using periodically textured metal films for light extraction from a semiconductor, using an angular emission argument [207]. The first experimental demonstration of such a solution was reported in 2005 by Pillai *et al.* [208], who showed a threefold enhancement over the full electroluminescence spectrum of a
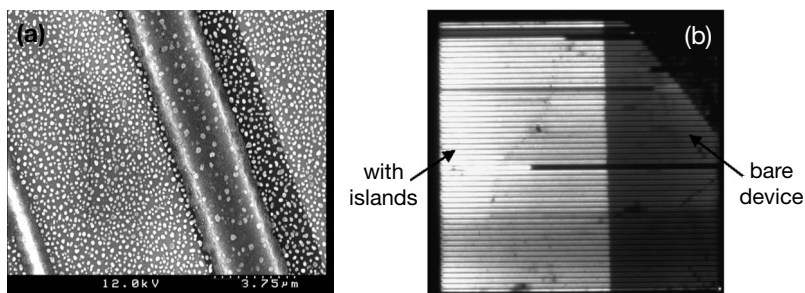
silicon emitter with silver nanoparticle islands on its surface. Figure 17, which shows a device partially covered with the islands, vividly illustrates the enhancement effect. After one year, they published an improvement to sevenfold enhancement [189]. Their analysis focuses on surface plasmon polaritons in the particles as a coupling mechanism between the incident and local fields. The particles function as a random array of transmitting optical antennas.

Optical antennas can also be used to enhance the efficiency of solid-state devices at wavelengths where we lack emission-efficient materials. Today's high-efficiency solid-state lighting devices use the remarkable properties of LEDs composed of InGaN and AlGaInP [209]. The former has a high emission yield in the blue–green spectral region [210], and the latter possesses a high emission efficiency in the red. For white light illumination one also requires emission in the green–yellow spectral region, but, unfortunately, InGaN turns out to have a low quantum efficiency in this region [211]. Near the peak sensitivity of the human eye (wavelength $\sim$550 nm) the external efficiency is only about 5%. Besides the low quantum efficiency in the green–yellow region, InGaN also possesses an efficiency roll-off at high electron–hole injection densities, limiting the performance of high-power LEDs. One avenue for increasing the emission yield in the green–yellow spectral region is the introduction of phosphors such as $Y_3Al_5O_{12}:Ce^{3+}$ (YAG) that are pumped by the blue emission of InGaN [212]. However, the introduction of phosphors brings other challenges such as saturation and photochemical stability.

Optical antennas in the form of nanoparticles with suitably engineered plasmonic modes are able to improve the efficiency of low quantum yield emitters and might prove beneficial in solid-state lighting applications. The improvements for a simple spherical nanoparticle antenna have been discussed in Subsection 3.6 (see Fig. 6), and much better efficiency enhancements can be expected for improved antenna geometries. Besides the potential for increasing quantum efficiencies, optical antennas might also enable higher extraction efficiencies by providing a means to extract photons from the source region.

All of these applications involve devices with inherently low efficiency. As shown in Subsection 3.6, antennas can only hurt devices with inherently high ef-

**Figure 17**



(a) Scanning electron microscope image of a silicon-on-insulator LED with silver nanoparticles on its surface. (b) Electroluminescence from an LED partially coated with silver nanoparticles. Brighter areas correspond to stronger electroluminescence intensity. Reprinted with permission from [208]. © 2008 American Institute of Physics.

ficiency. The limitations of metallic nanoparticles in light-emitting devices are pointed out by Sun *et al.* [213]. They consider an InGaN/GaN active quantum well in a dielectric medium and model the luminescence with and without a silver nanosphere. Their goal is to optimize the emitter–nanosphere separation and the size of the nanosphere. Finding a result similar to Eq. (14), Sun *et al.* thus conclude that nanoparticle antennas may be useful for detection and instrumentation, but that they hold little promise for efficient, large-area emitters.

Optical antennas may make low-cost but inefficient devices like OLEDs and silicon LEDs feasible, and they offer a way to patch up missing colors in efficient solid-state lighting. Developments in these directions are underway in various laboratories, and it will be interesting to see in which applications the optical antenna concept ultimately finds use.

## 4.4. Antennas for Coherent Control

So far we have discussed the ability of optical antennas to couple propagating far fields to localized near fields and vice versa, but we have ignored their interesting temporal dynamics. The broad spectral response associated with plasmons in metals corresponds to dynamics in the range of hundreds of attoseconds [214], which makes optical antennas useful tools for ultrafast applications like nanoscale computing, time-resolved spectroscopy, or selective chemical bonding. In short, the rapid response of the free-electron gas in a metal provides a means for controlling the dynamics of a system on the quantum level. Quantum control has been an active area of research recently, and many strategies have been suggested [215–219]. Ultrafast plasmonics is particularly promising, but it requires the ability to control local field distributions temporally and spatially.

### Figure 18
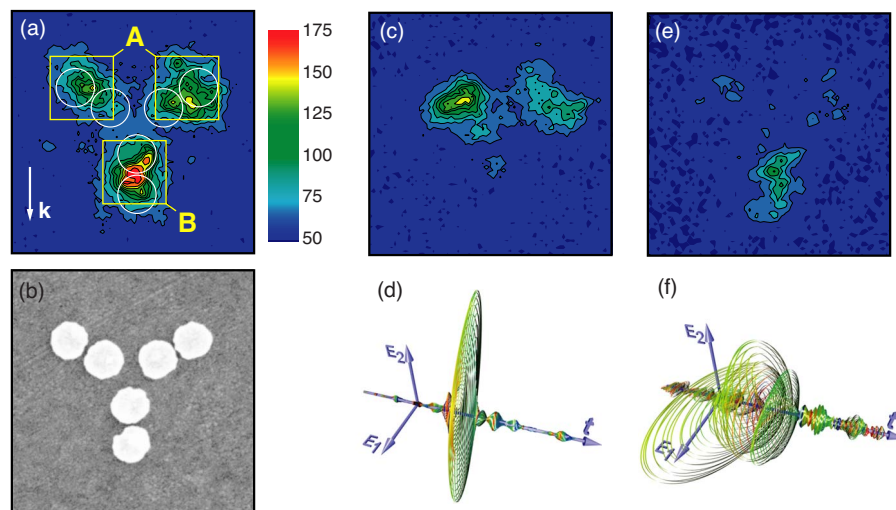


Coherent control of photoelectron generation in an optical antenna structure. (a) Photoelectron distribution for an incident *p*-polarized pulse with no coherent control. (b) Electron micrograph of the test structure. (c) Photoelectron distribution for excitation pulse shown in (d). (e) Photoelectron distribution for excitation pulse shown in (f). Adapted from [225] by permission from Macmillan Publishers Ltd., *Nature*, © 2007.

The antenna properties of metal nanostructures provide a convenient way to control plasmon dynamics. A pulse of light incident on a nanostructure imprints temporally dependent amplitude, phase, and polarization information on the structure. Stockman *et al.* showed that ultrafast pulse shaping can achieve many degrees of freedom to control the fields associated with the surface plasmons [220–222]. Three main strategies are used to achieve the desired control of surface plasmon oscillations. First, if the Green's function of the plasmonic system is known exactly, the incident field parameters can be solved for. Stockman showed that the Green's function has separable dependencies on geometry and material properties [222] and can in principle be calculated. Second, time-reversal techniques provide a way to concentrate fields to an arbitrary pattern in a sample without cumbersome calculations [222]. Using this method, model emitters (i.e. fluorescent dipoles) generate plasmons in the antenna structure, which then radiate into the near and far field. If these fields are recorded, they can be time reversed and played back, thus reconstructing the original excitation. One serious challenge associated with time-reversal approaches is that the near field, which contains essential reconstruction information, is difficult to measure, owing to its exponential distance dependence. But since the plasmons are relatively long lived, the antenna serves as a reverberating structure, slowly emitting energy into the far field to be recorded. Finally, if the system is configured in a feedback loop, learning algorithms can be used to find the optimal pulse shapes and polarizations for the desired effects [223,224]. This method was used recently in the first experimental demonstration of dynamic localization of surface plasmon fields in an antenna-type nanostructure by Aeschlimann *et al.* [225]. As illustrated in Fig. 18, photoelectron maximization and minimization leads to localization in different regions of the nanostructure. These experiments prove that the electromagnetic modes of an optical antenna can be controlled in time and space by pulsed laser excitation.

Applications such as nanoscale sensing, high-resolution spectroscopy, and optical logic require strongly confined and enhanced fields [222], and the possibility to coherently control the electromagnetic response of an optical antenna opens the door to temporally and spatially influence these fields.

## 5. Conclusions and Outlook

The study of optical antennas is still in its infancy. While some properties directly derive from classical antenna theory, the direct downscaling of antenna designs into the optical regime is not possible because radiation penetrates into metals and gives rise to plasma oscillations. In general, an optical antenna is designed to increase the interaction area of a local absorber or emitter with free radiation, thereby making the light–matter interaction more efficient. This is accounted for in quantities such as the LDOS, the antenna impedance, or the antenna aperture.

As in canonical antenna theory, there is no universal antenna design. Instead, optical antennas have to be optimized separately for each application. However, to achieve the best efficiency the internal energy dissipation of any antenna must be minimized. For a quantum emitter such as an atom, molecule, or ion, a good antenna yields a low nonradiative decay rate.

So far, most of the progress in fabrication of the more complicated antenna designs has been in the IR, where electron-beam lithography is relatively common-

place. Fabrication and testing at visible wavelengths is in its beginning states, but shows promise.

New ideas and developments are emerging at a rapid pace, and it is clear that the optical antenna concept will provide new opportunities for optoelectronic architectures and devices. Today, the building blocks for optical antennas are plasmonic nanostructures. These can be fabricated from the bottom up by colloidal chemistry or from the top down with established nanofabrication techniques, such as electron-beam lithography or focused ion-beam milling. It is also conceivable that future optical antenna designs will draw inspiration from biological systems such as light harvesting proteins in photosynthesis.

## Acknowledgments

## References

1. ISO Standard ISO/TS 27687, TC 229 (ISO, 2008).
2. Aristotle, *De Animalibus*, Theodorus Gaza, trans. (Johannes de Colonia and Johannes Manthen, 1476).
3. Aristotle, *History of Animals* (c. 340 B.C.E.).
4. T. G. Tucker, "Antemna, antenna," in *A Concise Etymological Dictionary of Latin* (Max Niemeyer Verlag, 1931), p. 19.
5. C. Watkins, "ten-," in *The American Heritage Dictionary of Indo-European Roots* (Houghton Mifflin, 2000), p. 90.
6. E. Klein, "Antenna," in *A Comprehensive Etymological Dictionary of the English Language* (Elsevier, 1966), p. 82.
7. J. A. Simpson and E. S. C. Weiner, "Antennas," in *The Oxford English Dictionary* (Oxford Univ. Press, 1989), p. 506.
8. F. E. Gardiol and Y. Fournier, "Salvan: cradle of wireless," Microwave J. **49**, 124–136 (2006).
9. W. P. Jolly, *Marconi* (Constable, 1972).
10. G. Marconi, "Wireless telegraphic communication," Nobel Lecture, December 11, 1909.
11. G. W. Pierce, "Experiments on resonance in wireless telegraph circuits," Phys. Rev. **19**, 196–217 (1904).
12. J. A. Fleming, "Telegraphy," *The New Volumes of the Encyclopedia Britannica*, 10th ed., vol. XXXIII (1902).
13. S. Walter, E. Bolmont, and A. Coret, "La correspondance entre Henri Poincaré et les physiciens, chimistes et ingénieurs," in *Publications of the Henri Poincaré Archives* (Birkhäuser, 2007), chap. 8.
14. A. Broca, *La télégraphie sans fils* (Gauthier Villars, 1899).
15. B. Franklin, in *The Papers of Benjamin Franklin*, L. W. Labaree, ed. (Yale Univ. Press, 1961), vol. 3, pp. 156–164.

16. M. C. H. E. Rodriguez-Garcia, "Systéme de télégraphie sans fil par ondes hertziennes," French Patent 301264 (June 14, 1900).

17. E. Ducretet, "Transmitting and receiving apparatus for Hertzian waves," U.S. Patent 726413 (April 28, 1903).

18. M. C. H. E. Rodriguez-Garcia, "Wireless telegraphy," U.S. Patent 795762 (July 25, 1905).

19. Antenna Standards Committee of the IEEE Antennas and Propagation Society, "IEEE standard definitions of terms for antennas," IEEE Std 145-1993 (IEEE, 1993).

20. L. Novotny, "The history of near-field optics," in *Progress in Optics*, E. Wolf, ed. (Elsevier, 2007), vol. 50, pp. 137–184.

21. *Nobel Lectures, Chemistry 1922–1941* (Elsevier, 1966).

22. J. Wessel, "Surface-enhanced optical microscopy," J. Opt. Soc. Am. B **2**, 1538–1540 (1985).

23. P. Anger, P. Bharadwaj, and L. Novotny, "Enhancement and quenching of single molecule fluorescence," Phys. Rev. Lett. **96**, 113002 (2006).

24. S. Kühn, U. Hakanson, L. Rogobete, and V. Sandoghdar, "Enhancement of single-molecule fluorescence using a gold nanoparticle as an optical nanoantenna," Phys. Rev. Lett. **97**, 017402 (2006).

25. G. Binnig and H. Rohrer, "Scanning tunneling microscopy," Helv. Phys. Acta **55**, 726–735 (1982).

26. M. Fleischmann, P. J. Hendra, and A. J. McQuillian, "Raman spectra of pyridine adsorbed at a silver electrode," Chem. Phys. Lett. **26**, 163–166 (1974).

27. D. L. Jeanmaire and R. P. V. Duyne, "Surface Raman spectroelectrochemistry: part I. Heterocyclic, aromatic, and aliphatic amines adsorbed on the anodized silver electrode," J. Electroanal. Chem. **84**, 1–20 (1977).

28. M. G. Albrecht and J. A. Creighton, "Anomalously intense Raman spectra of pyridine at a silver electrode," J. Am. Chem. Soc. **99**, 5215–5217 (1977).

29. J. Gersten and A. Nitzan, "Electromagnetic theory of enhanced Raman scattering of molecules adsorbed on rough surfaces," J. Chem. Phys. **73**, 3023–3037 (1980).

30. A. Wokaun, J. Gordon, and P. Liao, "Radiation damping in surface-enhanced Raman scattering," Phys. Rev. Lett. **48**, 957–960 (1982).

31. A. D. Boardman, ed., *Electromagnetic Surface Modes* (Wiley, 1982).

32. H. Metiu, *Surface Enhanced Spectroscopy*, vol. 17 of Progress in Surface Science, I. Prigogine and S. A. Rice, eds. (Pergamon, 1984), pp. 153–320.

33. M. Meier, A. Wokaun, and P. F. Liao, "Enhanced fields on rough surfaces: dipolar interactions among particles of sizes exceeding the Raleigh limit," J. Opt. Soc. Am. B **2**, 931–949 (1985).

34. U. C. Fischer and D. W. Pohl, "Observation on single-particle plasmons by near-field optical microscopy," Phys. Rev. Lett. **62**, 458–461 (1989).

35. J. Jackson, S. Westcott, L. Hirsch, J. West, and N. Halas, "Controlling the surface enhanced Raman effect via the nanoshell geometry," Appl. Phys. Lett. **82**, 257–259 (2003).

36. E. Prodan, C. Radloff, N. J. Halas, and P. Nordlander, "A hybridization model for the plasmon response of complex nanostructures," Science **320**, 419–422 (2003).

37. L. Novotny, R. X. Bian, and X. S. Xie, "Theory of nanometric optical tweezers," Phys. Rev. Lett. **79**, 645–648 (1997).

38. L. Novotny, E. J. Sanchez, and X. S. Xie, "Near-field optical imaging using

metal tips illuminated by higher-order Hermite–Gaussian beams," Ultramicroscopy **71**, 21–29 (1998).

39. L. O. Hocker, D. R. Sokoloff, A. S. V. Daneu, and A. Javan, "Frequency mixing in the infrared and far-infrared using metal-to-metal point contact diode," Appl. Phys. Lett. **12**, 401–402 (1968).

40. L. M. Matarrese and K. M. Evenson, "Improved coupling to infrared whisker diodes by use of antenna theory," Appl. Phys. Lett. **17**, 8–10 (1970).

41. A. Kirschke and K. Rothammel, *Rothammels Antennenbuch* (DARC Verlag, 2001).

42. G. Boreman, "Infrared microantennas," Proc. SPIE **3110**, 882–885 (1997).

43. J. Alda, J. Rico-García, J. López-Alonso, and G. Boreman, "Optical antennas for nano-photonic applications," Nanotechnology **16**, S230–S234 (2005).

44. F. González and G. Boreman, "Comparison of dipole, bowtie, spiral and log-periodic IR antennas," Infrared Phys. Technol. **146**, 418–428 (2004).

45. C. Fumeaux, G. Boreman, W. Herrmann, H. Rothuizen, and F. Kneubühl, "Polarization response of asymmetric-spiral infrared antennas," Appl. Opt. **36**, 6485–6490 (1997).

46. I. Codreanu and G. D. Boreman, "Infrared microstrip dipole antennas—FDTD predictions versus experiment," Microwave Opt. Technol. Lett. **29**, 381–383 (2001).

47. C. Middlebrook, P. Krenz, B. Lail, and G. Boreman, "Infrared phased-array antenna," Microwave Opt. Technol. Lett. **50**, 719–723 (2008).

48. R. D. Grober, R. J. Schoelkopf, and D. E. Prober, "Optical antenna: towards a unity efficiency near-field optical probe," Appl. Phys. Lett. **70**, 1354–1356 (1997).

49. D. W. Pohl, "Near-field optics seen as an antenna problem," in *Near-field Optics, Principles and Applications*, X. Zhu and M. Ohtsu, eds. (World Scientific, 2000), pp. 9–21.

50. L. Allen and J. H. Eberly, *Optical Resonance and Two-level Atoms* (Dover Publications, Inc., Mineola, NY, 1987).

51. L. Novotny and B. Hecht, *Principles of Nano-Optics* (Cambridge Univ. Press, 2006).

52. K. Joulain, R. Carminati, J. P. Mulet, and J. J. Greffet, "Definition and measurement of the local density of electromagnetic states close to an interface," Phys. Rev. B **68**, 245405 (2003).

53. E. M. Purcell, "Spontaneous emission probabilities at radio frequencies," Phys. Rev. **69**, 681 (1946).

54. K. H. Drexhage, M. Fleck, F. Shäfer, and W. Sperling, "Beeinflussung der Fluoreszenz eines Europium-chelates durch einen Spiegel," Ber. Bunsenges. Phys. Chem. **20**, 1179 (1966).

55. D. Kleppner, "Inhibited spontaneous emission," Phys. Rev. Lett. **47**, 233–236 (1981).

56. P. Goy, J. Raimond, M. Gross, and S. Haroche, "Observation of cavity-enhanced single-atom spontaneous emission," Phys. Rev. Lett. **50**, 1903–1906 (1983).

57. M. A. Wilson, P. Bushev, J. Eschner, F. Schmidt-Kaler, C. Becher, R. Blatt, and U. Dorner, "Vacuum-field level shifts in a single trapped ion mediated by a single distant mirror," Phys. Rev. Lett. **91**, 213602 (2003).

58. O. Labeau, P. Tamarat, H. Courtois, G. S. Agarwal, and B. Lounis, "Laser-induced resonance shifts of single molecules self-coupled by a metallic surface," Phys. Rev. Lett. **98**, 143003 (2007).

59. L. Novotny and S. J. Stranick, "Near-field optical microscopy and spectroscopy with pointed probes," Annu. Rev. Phys. Chem. **57**, 303–331 (2006).

60. J.-J. Greffet, Institut d'Optique, Paris, France (personal communication, 2008).

61. T. H. Taminiau R. J. Moerland, F. B. Segerink, L. Kuipers, and N. F. van Hulst, "λ/4 Resonance of an optical monopole antenna probed by single molecule fluorescence," Nano Lett. **7**, 28–33 (2007).

62. T. H. Taminiau, F. D. Stefani, F. B. Segerink, and N. F. van Hulst, "Optical antennas direct single-molecule emission," Nat. Photonics **2**, 234–237 (2008).

63. R. J. Moerland, N. F. van Hulst, H. Gersen, and L. Kuipers, "Probing the negative permittivity perfect lens at optical frequencies using near-field optics and single molecule detection," Opt. Eng. **13**, 1604–1614 (2005).

64. H. Gersen, M. F. García-Parajó, L. Novotny, J. A. Veerman, L. Kuipers, and N. F. van Hulst, "Influencing the angular emission of a single molecule," Phys. Rev. Lett. **85**, 5312 (2000).

65. C. Huang, A. Bouhelier, G. C. des Francs, A. Bruyant, A. Guenot, E. Finot, J.-C. Weeber, and A. Dereux, "Gain, detuning, and radiation patterns of nanoparticle optical antennas," Phys. Rev. B **78**, 155407 (2008).

66. R. Carminati, M. Nieto-Vesperinas, and J.-J. Greffet, "Reciprocity of evanescent electromagnetic waves," J. Opt. Soc. Am. A **15**, 706–712 (1998).

67. T. H. Taminiau, F. D. Stefani, and N. F. van Hulst, "Enhanced directional excitation and emission of single emitters by a nano-optical Yagi-Uda antenna," Opt. Express **16**, 10858–10866 (2008).

68. T. H. Taminiau and N. F. Van Hulst, ICFO—The Institute of Photonic Sciences, Castelldefels (Barcelona), Spain (personal communication, 2008).

69. K. T. Shimizu, W. K. Woo, B. R. Fisher, H. J. Eisler, and M. G. Bawendi, "Surface-enhanced emission from single semiconductor nanocrystals," Phys. Rev. Lett. **89**, 117401 (2002).

70. J. N. Farahani, D. W. Pohl, H.-J. Eisler, and B. Hecht, "Single quantum dot coupled to a scanning optical antenna: a tunable superemitter," Phys. Rev. Lett. **95**, 017402 (2005).

71. P. Bharadwaj and L. Novotny, "Spectral dependence of single molecule fluorescence enhancement," Opt. Express **15**, 14266–14274 (2007).

72. R. Loudon, *The Quantum Theory of Light*, 2nd ed., Oxford Science Publications (Clarendon, 1983).

73. L. Tang, S. E. Kocabas, S. Latif, A. K. Okyay, D.-S. Ly-Gagnon, K. C. Saraswat, and D. A. B. Miller, "Nanometre-scale germanium photodetector enhanced by a near-infrared dipole antenna," Nat. Photonics **2**, 226–229 (2008).

74. H. Xu, E. J. Bjernfeld, M. Käll, and L. Börjesson, "Spectroscopy of single hemoglobin molecules by surface enhanced Raman scattering," Phys. Rev. Lett. **83**, 4357–4360 (1999).

75. K. Li, M. I. Stockman, and D. J. Bergman, "Self-similar chain of metal nanospheres as an efficient nanolens," Phys. Rev. Lett. **91**, 227402 (2003).

76. T. Kalkbrenner, U. Håkanson, A. Schädle, S. Burger, C. Henkel, and V. Sandoghdar, "Optical microscopy via spectral modifications of a nanoantenna," Phys. Rev. Lett. **95**, 200801 (2005).

77. P. Bharadwaj, P. Anger, and L. Novotny, "Nanoplasmonic enhancement of single-molecule fluorescence," Nanotechnology **18**, 044017 (2007).

78. G. W. Ford and W. H. Weber, "Electromagnetic interactions of molecules with metal surfaces," Phys. Rep. **113**, 195–287 (1984).

79. V. V. Klimov, M. Ducloy, and V. S. Letokhov, "Spontaneous emission in the presence of nanobodies," Quantum Electron. **31**, 569–586 (2001).

80. V. V. Klimov and V. S. Letokhov, "Electric and magnetic dipole transitions of an atom in the presence of spherical dielectric interface," Laser Phys. **15**, 61–73 (2005).

81. A. Wokaun, H.-P. Lutz, A. P. King, U. P. Wild, and R. R. Ernst, "Energy transfer in surface enhanced luminescence," J. Chem. Phys. **79**, 509–514 (1983).

82. L. Novotny, "Effective wavelength scaling for optical antennas," Phys. Rev. Lett. **98**, 266802 (2007).

83. G. W. Bryant, F. J. G. de Abajó, and J. Aizpurua, "Mapping the plasmon resonances of metallic nanoantennas," Nano Lett. **8**, 631–636 (2008).

84. P. J. Burke, S. Li, and Z. Yu, "Quantitative theory of nanowire and nanotube antenna performance," IEEE Trans. Nanotech. **5**, 314–334 (2006).

85. A. Alù and N. Engheta, "Input impedance, nanocircuit loading, and radiation tuning of optical nanoantennas," Phys. Rev. Lett. **101**, 043901 (2008).

86. V. M. Shalaev, "Electromagnetic properties of small-particle composites," Phys. Rep. **272**, 61–137 (1996).

87. M. R. Beversluis, A. Bouhelier, and L. Novotny, "Continum generation from single gold nanostructures through near-field mediated intraband transitions," Phys. Rev. B **68**, 115433 (2003).

88. J. R. Zurita-Sanchez and L. Novotny, "Multipolar interband absorption in a semiconductor quantum dot. I. Electric quadrupole enhancement," J. Opt. Soc. Am. B **19**, 1355–1362 (2002).

89. J. R. Zurita-Sanchez and L. Novotny, "Multipolar interband absorption in a semiconductor quantum dot. II. Magnetic dipole enhancement," J. Opt. Soc. Am. B **19**, 2722–2726 (2002).

90. I. A. Larkin, M. I. Stockman, M. Achermann, and V. I. Klimov, "Dipolar emitters at nanoscale proximity of metal surfaces: giant enhancement of relaxation," Phys. Rev. B **69**, 121403(R) (2004).

91. J. Aizpurua and A. Rivacoba, "Nonlocal effects in the plasmons of nanowires and nanocavities excited by fast electron beams," Phys. Rev. B **78**, 035404 (2008).

92. F. J. G. de Abajó, "Nonlocal effects in the plasmons of strongly interacting nanoparticles, dimers, and waveguides," J. Phys. Chem. C **112**, 17983–17987 (2008).

93. J. Zuloaga, E. Prodan, and P. Nordlander, "Quantum description of the plasmon resonances of a nanoparticle dimer," Nano Lett. **9**, 88789 (2009).

94. R. A. Ganeev, I. A. Kulagin, A. I. Ryasnyansky, R. I. Tugushev, and T. Usmanov, "Characterization of nonlinear optical parameters of KDP, LiNb$o_3$ and BBO crystals," Opt. Commun. **229**, 403–412 (2003).

95. N. Bloembergen, W. K. Burns, and M. Matsuoka, "Reflected third harmonic generation by picosecond laser pulses," Opt. Commun. **1**, 195–198 (1969).

96. J. Renger, R. Quidant, N. V. Hulst, and L. Novotny, "Optical four-wave mixing at planar noble metal surfaces," submitted to Phys. Rev. Lett..

97. A. Bouhelier, M. Beversluis, A. Hartschuh, and L. Novotny, "Near-field second-harmonic generation induced by local field enhancement," Phys. Rev. Lett. **90**, 013903 (2003).

98. M. Labardi, M. Allegrini, M. Zavelani-Rossi, D. Polli, G. Cerullo, S. D. Silvestri, and O. Svelto, "Highly efficient second-harmonic nanosource for near-field optics and microscopy," Opt. Lett. **29**, 62–64 (2004).

99. M. Lippitz, M. A. van Dijk, and M. Orrit, "Third-harmonic generation from single gold nanoparticles," Nano Lett. **5**, 799 (2005).

100. A. Bouhelier, M. R. Beversluis, and L. Novotny, "Characterization of nanoplasmonic structures by locally excited photoluminescence," Appl. Phys. Lett. **83**, 5041–5043 (2003).

101. P. Schuck, D. P. Fromm, A. Sundaramurthy, G. S. Kino, and W. E. Moerner, "Improving the mismatch between light and nanoscale objects with gold bowtie nanoantennas," Phys. Rev. Lett. **94**, 017402 (2005).

102. P. Ghenuche, S. Cherukulappurath, T. H. Taminiau, N. F. van Hulst, and R. Quidant, "Spectroscopic mode mapping of resonant plasmon nanoantennas," Phys. Rev. Lett. **101**, 116805 (2008).

103. M. Danckwerts and L. Novotny, "Optical frequency mixing at coupled gold nanoparticles," Phys. Rev. Lett. **98**, 026104 (2007).

104. S. Palomba and L. Novotny, "Nonlinear excitation of surface plasmon polaritons by four-wave mixing," Phys. Rev. Lett. **101**, 056802 (2008).

105. S. Palomba, M. Danckwerts, and L. Novotny, "Nonlinear plasmonics with gold nanoparticle antennas," submitted to J. Opt. A, Pure Appl. Opt..

106. D. E. Chang, A. S. Sørensen, E. A. Demler, and M. D. Lukin, "A single-photon transistor using nanoscale surface plasmons," Nat. Phys. **3**, 807–812 (2007).

107. R. M. Bakker, A. Boltasseva, Z. Liu, R. H. Pedersen, S. Gresillon, A. V. Kildishev, V. P. Drachev, and V. M. Shalaev, "Near-field excitation of nanoantenna resonance," Opt. Express **15**, 13682–13688 (2006).

108. F. Neubrech, T. Kolb, R. Lovrincic, G. Fahsold, A. Pucci, J. Aizpurua, T. W. Cornelius, M. E. Toimil-Molares, R. Neumann, and S. Karim, "Resonances of individual metal nanowires in the infrared," Appl. Phys. Lett. **89**, 253104 (2006).

109. T. Søndergaard and S. I. Bozhevolnyi, "Metal nano-strip optical resonators," Opt. Express **15**, 4198–4204 (2007).

110. T. Søndergaard, J. Beermann, A. Boltasseva, and S. I. Bozhevolnyi, "Slow-plasmon resonant-nanostrip antennas: analysis and demonstration," Phys. Rev. B **77**, 011520 (2008).

111. J. Jung, T. Søndergaard, J. Beermann, A. Boltasseva, and S. I. Bozhevolnyi, "Theoretical analysis and experimental demonstration of resonant light scattering from metal nanostrips on quartz," J. Opt. Soc. Am. B **26**, 121–124 (2009).

112. T. Laroche and C. Girard, "Near-field optical properties of single plasmonic nanowires," Appl. Phys. Lett. **89**, 233119 (2006).

113. S. A. Maier, "Plasmonic field enhancement and SERS in the effective mode volume picture," Opt. Express **14**, 1957–1964 (2006).

114. E. S. Barnard, J. S. White, A. Chandran, and M. L. Brongersma, "Spectral properties of plasmonic resonator antennas," Opt. Express **16**, 16529–16537 (2006).

115. A. Hohenau, J. R. Krenn, G. Schider, H. Ditlbacher, A. Leitner, F. R. Aussenegg, and W. L. Schaich, "Optical near-field of multipolar plasmons of rod-shaped gold nanoparticles," Europhys. Lett. **69**, 538–543 (2005).

116. H. Ditlbacher, J. R. Krenn, N. Felidj, B. Lamprecht, G. Schider, M. Salerno, A. Leitner, and F. R. Aussenegg, "Silver nanowires as surface plasmon resonators," Phys. Rev. Lett. **95**, 257403 (2005).

117. N. Yu, L. Diehl, E. Cubukcu, C. Pflügl, D. Bour, S. Corzine, J. Zhu, G. Höfler, K. B. Crozier, and F. Capasso, "Near-field imaging of quantum cascade laser transverse modes," Opt. Express **15**, 13227–13235 (2007).

118. R. L. Olmon, P. M. Krenz, A. C. Jones, G. D. Boreman, and M. B. Raschke, "Near-field imaging of optical antenna modes in the mid-infrared," Opt. Express **16**, 20295–20305 (2008).

119. J. Nelayah, M. Kociak, O. Stéphan, F. J. G. de Abajo, M. Tencé, L. Henrard, D. Taverna, I. Pastoriza-Santos, L. M. Liz-Marzán, and C. Colliex, "Mapping surface plasmons on a single metallic nanoparticle," Nat. Phys. **3**, 348–353 (2007).

120. F. J. G. de Abajó and M. Kociak, "Probing the photonic local density of states with electron energy loss spectroscopy," Phys. Rev. Lett. **100**, 106804 (2008).

121. K. B. Crozier, A. Sundaramurthy, G. S. Kino, and C. F. Quate, "Optical antennas: resonators for local field enhancement," J. Appl. Phys. **94**, 4632–4642 (2003).

122. A. Sundaramurthy, K. B. Crozier, G. S. Kino, D. P. Fromm, P. J. Schuck, and W. E. Moerner, "Field enhancement and gap-dependent resonance in a system of two opposing tip-to-tip Au nanotriangles," Phys. Rev. B **72**, 165409 (2005).

123. P. Mühlschlegel, H.-J. Eisler, O. J. F. Martin, B. Hecht, and D. W. Pohl, "Resonant optical antennas," Science **308**, 1607–1609 (2005).

124. A. Alù and N. Engheta, "Hertzian plasmonic nanodimer as an efficient optical nanoantenna," Phys. Rev. B **78**, 195111 (2008).

125. A. Alù and N. Engheta, "Tuning the scattering response of optical nanoantennas with nanocircuit loads," Nat. Photonics **2**, 307–310 (2008).

126. J. Sun, S. Carney, and J. Schotland, "Strong tip effects in near-field optical tomography," J. Appl. Phys. **102**, 103103 (2007).

127. E. Cubukcu, E. A. Kort, K. B. Crozier, and F. Capasso, "Plasmonic laser antenna," Appl. Phys. Lett. **89**, 093120 (2006).

128. A. Hartschuh, M. R. Beversluis, A. Bouhelier, and L. Novotny, "Tip-enhanced optical spectroscopy," Philos. Trans. R. Soc. London, Ser. A **362**, 807–819 (2003).

129. A. Hartschuh, "Tip-enhanced near-field optical microscopy," Angew. Chem., Int. Ed. **47**, 8178–8191 (2008).

130. E. Bailo and V. Deckert, "Tip-enhanced Raman scattering," Chem. Soc. Rev. **37**, 921–930 (2008).

131. E. Fort and S. Grésillon, "Surface enhanced fluorescence," J. Phys. D **41**, 013001 (2008).

132. R. Bachelot, P. Gleyzes, and A. C. Boccara, "Near-field optical microscope based on local perturbation of a diffraction spot," Opt. Lett. **20**, 1924–1926 (1995).

133. S. Kawata and Y. Inouye, "Scanning probe optical microscopy using a metallic probe tip," Ultramicroscopy **57**, 313–317 (1995).

134. B. Deutsch, R. Hillenbrand, and L. Novotny, "Near-field amplitude and phase recovery using phase-shifting interferometry," Opt. Express **16**, 494–501 (2008).

135. R. Vogelgesang, J. Dorfmüller, R. Esteban, R. T. Weitz, A. Dmitriev, and K. Kern, "Plasmonic nanostructures in aperture-less scanning near-field optical microscopy (aSNOM)," Phys. Status Solidi B **245**, 2255–2260 (2008).

136. A. Cvitkovic, N. Ocelic, J. Aizpurua, R. Guckenberger, and R. Hillenbrand, "Infrared imaging of single nanoparticles via strong field enhancement in a scanning nanogap," Phys. Rev. Lett. **97**, 060801 (2006).

137. B. Knoll and F. Keilmann, "Enhanced dielectric contrast in scattering-type

scanning near-field optical microscopy," Opt. Commun. **182**, 321–328 (2000).

138. R. Hillenbrand and F. Keilmann, "Complex optical constants on a sub-wavelength scale," Phys. Rev. Lett. **85**, 3029–3032 (2000).

139. F. Keilmann and R. Hillenbrand, "Near-field microscopy by elastic light scattering from a tip," Philos. Trans. R. Soc. London, Ser. A **362**, 787–797 (2004).

140. M. Wenzel, T. Härtling, P. Olk, S. C. Kehr, S. Grafström, S. Winnerl, M. Helm, and L. M. Eng, "Gold nanoparticle tips for optical field confinement in infrared scattering near-field optical microscopy," Opt. Express **16**, 12302–12312 (2008).

141. X. S. Xie and J. K. Trautman, "Optical studies of single molecules at room temperature," Annu. Rev. Phys. Chem. **49**, 441–480 (1998).

142. J. R. Lakowicz, J. Malicka, I. Gryczynski, Z. Gryczynski, and C. D. Geddes, "Radiative decay engineering: the role of photonic mode density in biotechnology," J. Phys. D **36**, R240–R249 (2003).

143. O. L. Muskens, V. Giannini, J. A. Sánchez-Gil, and J. G. Rivas, "Strong enhancement of the radiative decay rate of emitters by single plasmonic nanoantennas," Nano Lett. **7**, 2871–2875 (2007).

144. H. Kuhn, "Classical aspects of energy transfer in molecular systems," J. Chem. Phys. **53**, 101–108 (1970).

145. R. R. Chance, A. Prock, and R. Silbey, "Lifetime of an emitting molecule near a partially reflecting surface," J. Chem. Phys. **60**, 2744–2748 (1974).

146. M. Thomas, J.-J. Greffet, R. Carminati, and J. R. Arias-Gonzalez, "Single-molecule spontaneous emission close to absorbing nanostructures," Appl. Phys. Lett. **85**, 3863–3865 (2004).

147. J. R. Lakowicz, "Radiative decay engineering 5: metal-enhanced fluorescence and plasmon emission," Anal. Biochem. **337**, 171–194 (2005).

148. A. Hartschuh, H. Qian, A. J. Meixner, N. Anderson, and L. Novotny, "Nanoscale optical imaging of excitons in single-walled carbon nanotubes," Nano Lett. **5**, 2310 (2005).

149. H. Qian, C. Georgi, N. Anderson, A. A. Green, M. C. Hersam, L. Novotny, and A. Hartschuh, "Exciton transfer and propagation in carbon nanotubes studied by near-field optical microscopy," Nano Lett. **8**, 1363–1367 (2008).

150. H. Qian, P. T. Araujo, C. Georgi, T. Gokus, N. Hartmann, A. A. Green, A. Jorio, M. C. Hersam, L. Novotny, and A. Hartschuh, "Visualizing the local optical response of semiconducting carbon nanotubes to DNA-wrapping," Nano Lett. **8**, 2706–2711 (2008).

151. F. Wang, G. Dukovic, L. E. Brus, and T. F. Heinz, "Time-resolved fluorescence of carbon nanotubes and its implication for radiative lifetimes," Phys. Rev. Lett. **92**, 177401 (2004).

152. F. Tam, G. P. Goodrich, B. R. Johnson, and N. J. Halas, "Plasmonic enhancement of molecular fluorescence," Nano Lett. **7**, 496501 (2007).

153. J. S. Biteen, N. Lewis, H. Atwater, H. Mertens, and A. Polman, "Spectral tuning of plasmon-enhanced silicon quantum dot luminescence," Appl. Phys. Lett. **88**, 131109 (2006).

154. H. Mertens, J. S. Biteen, H. A. Atwater, and A. Polman, "Polarization-selective plasmon-enhanced silicon quantum-dot luminescence," Nano Lett. **6**, 2622–2625 (2006).

155. N. A. Issa and R. Guckenberger, "Fluorescence near metal tips: the roles of

energy transfer and surface plasmon polaritons," Opt. Express **15**, 12131–12144 (2007).

156. Y. Chen, K. Munechika, and D. S. Ginger, "Dependence of fluorescence intensity on the spectral overlap between fluorophores and plasmon resonant single silver nanoparticles," Nano Lett. **7**, 690–696 (2007).

157. Y. Chen, K. Munechika, I. J.-L. Plante, A. M. Munro, S. E. Skrabalak, Y. Xia, and D. S. Ginger, "Excitation enhancement of CdSe quantum dots by single metal nanoparticles," Appl. Phys. Lett. **93**, 053106 (2008).

158. M. F. Garcia-Parajo, "Optical antennas focus in on biology," Nat. Photonics **2**, 201–203 (2008).

159. C. Höppener and L. Novotny, "Antenna-based optical imaging of single $Ca^{2+}$ transmembrane proteins in liquids," Nano Lett. **8**, 642–646 (2008).

160. C. Höppener and L. Novotny, "Imaging of membrane proteins using antenna-based optical microscopy," Nanotechnology **19**, 384012 (2008).

161. H. Frey, F. Keilmann, A. Kriele, and R. Guckenberger, "Enhancing the resolution of scanning near-field optical microscopy by a metal tip grown on an aperture probe," Appl. Phys. Lett. **81**, 5530–5532 (2002).

162. H. G. Frey, S. Witt, K. Felderer, and R. Guckenberger, "High-resolution imaging of single fluorescent molecules with the optical near-field of a metal tip," Phys. Rev. Lett. **93**, 200801 (2004).

163. R. Esteban, M. Laroche, and J.-J. Greffet, "Influence of metallic nanoparticles on upconversion processes," J. Appl. Phys. **105**, 033107 (2009).

164. S. Nie and S. R. Emory, "Probing single molecules and single nanoparticles by surface enhanced Raman scattering," Science **275**, 1102 (1997).

165. K. Kneipp, Y. Wang, H. Kneipp, I. Itzkan, R. R. Dasary, and M. S. Feld, "Single molecule detection using surface enhanced Raman scattering (SERS)," Phys. Rev. Lett. **78**, 1667–1670 (1997).

166. A. M. Michaels, J. Jiang, and L. Brus, "Ag nanocrystal junctions as the site for surface-enhanced Raman scattering of single Rhodamine 6G molecules," J. Phys. C **104**, 11965–11971 (2000).

167. M. Moskovits, "Surface-enhanced Raman spectroscopy: a brief retrospective," J. Raman Spectrosc. **36**, 485–496 (2005).

168. D. P. Fromm, A. Sundaramurthy, A. Kinkhabwala, P. J. Schuck, G. S. Kino, and W. E. Moerner, "Exploring the chemical enhancement for surface-enhanced Raman scattering with Au bowtie nanoantennas," J. Chem. Phys. **124**, 061101 (2006).

169. R. M. Stöckle, Y. D. Suh, V. Deckert, and R. Zenobi, "Nanoscale chemical analysis by tip-enhanced Raman spectroscopy," Chem. Phys. Lett. **318**, 131–136 (2000).

170. A. Hartschuh, E. Sanchez, X. Xie, and L. Novotny, "High-resolution near-field Raman microscopy of single-walled carbon nanotubes," Phys. Rev. Lett. **90**, 095503 (2003).

171. A. Hartschuh, H. Qian, A. J. Meixner, N. Anderson, and L. Novotny, "Tip-enhanced optical spectroscopy of single-walled carbon nanotubes," in *Tip Enhancement*, S. Kawata and V. M. Shalaev, eds., Advances in Nano-Optics and Nano-Photonics (Elsevier, 2007), pp. 157–176.

172. N. Anderson, A. Hartschuh, and L. Novotny, "Chirality changes in carbon nanotubes studied with near-field Raman spectroscopy," Nano Lett. **7**, 577–582 (2007).

173. A. Rasmussen and V. Deckert, "Surface- and tip-enhanced Raman scattering of DNA components," J. Raman Spectrosc. **37**, 311–317 (2006).

174. U. Neugebauer, P. Rösch, M. Schmitt, J. Popp, C. Julien, A. Rasmussen, C.

Budich, and V. Deckert, "On the way to nanometer-sized information of the bacterial surface by tip-enhanced Raman spectroscopy," ChemPhysChem **7**, 1428–1430 (2006).

175. J. Steidtner and B. Pettinger, "Tip-enhanced Raman spectroscopy and microscopy on single dye molecules with 15 nm resolution," Phys. Rev. Lett. **100**, 236101 (2008).

176. C. C. Neacsu, J. Dreyer, N. Behr, and M. B. Raschke, "Scanning-probe Raman spectroscopy with single-molecule sensitivity," Phys. Rev. B **73**, 193406 (2006).

177. W. Zhang, B. S. Yeo, T. Schmid, and R. Zenobi, "Single molecule tip-enhanced Raman spectroscopy with silver tips," J. Phys. Chem. C **111**, 1733–1738 (2007).

178. W. C. Brown, "The history of power transmission by radio waves," IEEE Trans. Microwave Theory Tech. **32**, 1230–1242 (1984).

179. R. L. Bailey, "A proposed new concept for a solar-energy convertor," J. Eng. Power **94**, 73–77 (1972).

180. A. M. Marks, "Device for conversion of light to electric power," U.S. Patent 4,445,050 (April 24, 1984).

181. A. M. Marks, "Ordered dipolar light-electric power converter," U.S. Patent 4,574,161 (March 4, 1986).

182. A. M. Marks, "Femto diode and applications," U.S. Patent 4,720,642 (January 19, 1988).

183. R. Corkish, M. A. Green, and T. Puzzer, "Solar energy collection by antennas," Sol. Energy **73**, 395–401 (2002).

184. K. Kempa, J. Rybczynski, Z. Huang, K. Gregorczyk, A. Vidan, B. Kimball, J. Carlson, G. Benham, Y. Wang, A. Herczynski, and Z. F. Ren, "Carbon nanotubes as optical antennae," Adv. Mater. (Weinheim, Ger.) **19**, 421–426 (2007).

185. C. Hägglund, "Nanoparticle plasmon influence on the charge carrier generation in solar cells," Ph.D. thesis, Chalmers University of Technology, Göteborg, Sweden (2008).

186. H. R. Stuart and D. G. Hall, "Absorption enhancement in silicon-on-insulator waveguides using metal island films," Appl. Phys. Lett. **69**, 2327–2329 (1996).

187. K. R. Catchpole and S. Pillai, "Absorption enhancement due to scattering by dipoles into silicon waveguides," J. Appl. Phys. **100**, 044504 (2006).

188. M. Kirkengen, J. Bergli, and Y. M. Galperin, "Direct generation of charge carriers in c-Si solar cells due to embedded nanoparticles," J. Appl. Phys. **102**, 093713 (2007).

189. S. Pillai, K. Catchpole, T. Trupke, and M. Green, "Surface plasmon enhanced silicon solar cells," J. Appl. Phys. **101**, 093105 (2007).

190. K. Nakayama, K. Tanabe, and H. A. Atwater, "Plasmonic nanoparticle enhanced light absorption in GaAs solar cells," Appl. Phys. Lett. **93**, 121904 (2008).

191. S. H. Lim, W. Mar, P. Matheu, D. Derkacs, and E. T. Yu, "Photocurrent spectroscopy of optical absorption enhancement in silicon photodiodes via scattering from surface plasmon polaritons in gold nanoparticles," J. Appl. Phys. **101**, 104309 (2007).

192. C. Hägglund, M. Zäch, G. Petersson, and B. Kasemo, "Electromagnetic coupling of light into a silicon solar cell by nanodisk plasmons," Appl. Phys. Lett. **92**, 053110 (2008).

193. A. J. Morfa, K. L. Rowlen, T. H. Reilly, M. J. Romero, and J. van de Lage-

maat, "Plasmon-enhanced solar energy conversion in organic bulk hetero-junction photovoltaics," Phys. Rev. E **92**, 013504 (2008).

194. S.-S. Kim, S.-I. Na, J. Jo, D.-Y. Kim, and Y.-C. Nah, "Plasmon enhanced performance of organic solar cells using electrodeposited Ag nanoparticles," Appl. Phys. Lett. **93**, 073307 (2008).

195. D. Derkacs, W. V. Chen, P. M. Matheu, S. H. Lim, P. K. L. Yu, and E. T. Yu, "Nanoparticle-induced light scattering for improved performance of quantum-well solar cells," Appl. Phys. Lett. **93**, 091107 (2008).

196. K. R. Catchpole and A. Polman, "Plasmonic solar cells," Opt. Express **16**, 21793–21800 (2008).

197. B. O'Regan and M. Grätzel, "A low-cost, high-efficiency solar cell based on dye-sensitized colloidal TiO$_2$ films," Nature **353**, 737–740 (1991).

198. G. Zhao, H. Kozuka, and T. Yoko, "Effects of the incorporation of silver and gold nanoparticles on the photoanodic properties of rose bengal sensitized TiO$_2$ film electrodes prepared by sol-gel method," Sol. Energy Mater. Sol. Cells **46**, 219–231 (1997).

199. C. Wen, K. Ishikawa, M. Kishima, and K. Yamada, "Effects of silver particles on the photovoltaic properties of dye-sensitized TiO$_2$ thin films," Sol. Energy Mater. Sol. Cells **61**, 339–351 (2000).

200. C. Hägglund, M. Zäch, and B. Kasemo, "Enhanced charge carrier generation in dye sensitized solar cells by nanoparticle plasmons," Appl. Phys. Lett. **92**, 013113 (2008).

201. H. Kozuka, G. Zhao, and T. Yoko, "Sol-gel preparation and photoelectrochemical properties of TiO$_2$ films containing Au and Ag metal particles," Thin Solid Films **277**, 147–154 (1996).

202. Y. Tian and T. Tatsuma, "Mechanisms and applications of plasmon-induced charge separation at TiO$_2$ films loaded with gold nanoparticles," J. Am. Chem. Soc. **127**, 7632–7637 (2005).

203. S. Wedge, J. A. E. Wasey, and W. L. Barnes, "Coupled surface plasmon-polariton mediated photoluminescence from a top-emitting organic light-emitting structure," Appl. Phys. Lett. **85**, 182–184 (2004).

204. C. Liu, V. Kamaev, and Z. V. Vardenya, "Efficiency enhancement of an organic light-emitting diode with a cathode forming two-dimensional periodic hole array," Appl. Phys. Lett. **86**, 143501 (2005).

205. E. Ozbay, "Plasmonics: merging photonics and electronics at nanoscale dimensions," Science **311**, 189–193 (2006).

206. P. Ball, "Let there be light," Nature **409**, 974–976 (2001).

207. W. Barnes, "Electromagnetic crystals for surface plasmon polaritons and the extraction of light from emissive devices," J. Lightwave Technol. **17**, 2170–2182 (1999).

208. S. Pillai, K. R. Catchpole, T. Trupke, G. Zhang, J. Zhao, and M. A. Green, "Enhanced emission from Si-based light emitting diodes using surface plasmons," Appl. Phys. Lett. **88**, 161102 (2006).

209. *Basic Research Needs for Solid-State Lighting*, Report of the Basic Energy Sciences Workshop on Solid-State Lighting (U.S. Department of Energy,2006), http://www.sc.doe.gov/bes/reports/files/SSL_rpt.pdf.

210. S. Nakamura, T. Mukai, and M. Senoh, "Candela-class high-brightness InGaN/AlGaN double-heterostructure blue-light-emitting diodes," Appl. Phys. Lett. **64**, 1687–1689 (1994).

211. C. Wetzel, T. Salagaj, T. Detchprohm, P. Li, and J. S. Nelson, "GaInN/GaN growth optimization for high power green light emitting diodes," Appl. Phys. Lett. **85**, 866–868 (2004).

212. P. Schlotter, R. Schmidt, and J. Schneider, "Luminescence conversion of blue light mmitting diodes," Appl. Phys. A **64**, 417 (1997).

213. J. Sun, J. Khurgin, and R. Soref, "Plasmonic light-emission enhancement with isolated metal nanoparticles and their coupled arrays," J. Opt. Soc. Am. B **25**, 1748–1755 (2008).

214. M. Stockman, M. Kling, U. Kleinberg, and F. Krausz, "Attosecond nanoplasmonic-field microscope," Nat. Photonics **1**, 539–544 (2007).

215. H. Rabitz, R. de Vivie-Riedle, M. Motzkus, and K. Kompa, "Whither the future of controlling quantum phenomena?" Science **288**, 824–828 (2000).

216. H. Rabitz, M. Hsieh, and C. Rosenthal, "Quantum optimally controlled transition landscapes," Science **303**, 1998–2001 (2004).

217. S. Shi, A. Woody, and H. Rabitz, "Optimal control of selective vibrational excitation in harmonic linear chain molecules," J. Chem. Phys. **88**, 6870–6883 (1988).

218. M. Stockman, D. Bergman, and T. Kobayashi, "Coherent control of nanoscale localization of ultrafast optical excitation in nanosystems," Phys. Rev. B **69**, 054202 (2004).

219. Z. Liu, H. Lee, Y. Xiong, C. Sun, and X. Zhang, "Far-field optical hyperlens magnifying sub-diffraction-limited objects," Science **315**, 1686 (2007).

220. M. I. Stockman, S. V. Faleev, and D. J. Bergman, "Coherently controlled femtosecond energy localization on nanoscale," Appl. Phys. B **74**, S63–S67 (2002).

221. M. I. Stockman, "Nanofocusing of optical energy in tapered plasmonic waveguides," Phys. Rev. Lett. **93**, 137404 (2004).

222. M. I. Stockman, "Ultrafast nanoplasmonics under coherent control," New J. Phys. **10**, 025031 (2008).

223. T. Brixner, F. G. de Abajo, J. Schneider, and W. Pfeiffer, "Nanoscopic ultrafast space-time-resolved spectroscopy," Phys. Rev. Lett. **95**, 093901 (2005).

224. M. Sukharev and T. Seideman, "Phase and polarization control as a route to plasmonic nanodevices," Nano Lett. **6**, 715–719 (2006).

225. M. Aeschlimann, M. Bauer, D. Bayer, T. Brixner, F. G. de Abajó, W. Pfeiffer, M. Rohmer, C. Spindler, and F. Steeb, "Adaptive subwavelength control of nano-optical fields," Nature **446**, 301–304 (2007).